A universal preservation protocol for multi-omic and histological analysis of kidney tissue

Sydney E. Gies[1,2,*,¶], Sonja Hänzelmann[1,2,3,4,¶], Dominik Kylies[1,2], Simon Lagies[5,6], Moritz Lassé[1,2], Fabian Hausmann[2,3,4], Robin Khatri[2,3,4], Manuela Poets[1,2,3,4], Tianran Zhang[2,3,4], Shun Lu[1,2], Shuya Liu[1,2], Silvia Chilla[1,2], Ilka Edenhofer[1,2], Jan Czogalla[1,2], Fabian Braun[1,2], Bernd Kammerer[5,7,8,9], Markus M. Rinschen[1,2,10,11], Victor G. Puelles[1,2, 12, 13], Stefan Bonn[2,3,4], Maja T. Lindenmeyer[1,2,&], Tobias B. Huber[1,2,&]

[1]III. Department of Medicine, University Medical Center Hamburg-Eppendorf, Hamburg, Germany

[2]Hamburg Center for Kidney Health, University Medical Center Hamburg-Eppendorf, Hamburg, Germany

[3]Center for Biomedical AI, University Medical Center Hamburg-Eppendorf, Hamburg, Germany

[4]Institute of Medical Systems Biology, University Medical Center Hamburg-Eppendorf, Hamburg, Germany

[5]Core Competence Metabolomics (Hilde-Mangold-Haus), University of Freiburg, 79104 Freiburg, Germany

[6]Institute of Medical Microbiology and Hygiene, Faculty of Medicine, Medical Center-University of Freiburg, Freiburg, Germany.

[7]Institute of Organic Chemistry, University of Freiburg, Freiburg, Germany

[8]BIOSS Centre for Biological Signaling Studies, University of Freiburg, Freiburg, Germany

[9]Spemann Graduate School of Biology and Medicine (SGBM), University of Freiburg, Freiburg, Germany

[10]Department of Biomedicine, Aarhus University, Aarhus, Denmark

[11]Aarhus Institute of Advanced Studies (AIAS), Aarhus, Denmark

[12]Department of Clinical Medicine, Aarhus University

[13]Department of Pathology, Aarhus University Hospital.

[¶],& These authors contributed equally.

[*]Correspondence:
Sydney E. Gies, MD
E-Mail: s.gies@uke.de
University Medical Center Hamburg Eppendorf
III. Department of Medicine
Martinistrasse 52
20246 Hamburg

Abstract

Biobanking of tissue from clinically obtained kidney biopsies for later use with multi-omic and imaging techniques is an inevitable step to overcome the need of disease model systems and towards translational medicine. Hence, collection protocols ensuring integration into daily clinical routines using preservation media not requiring liquid nitrogen but instantly preserving kidney tissue for clinical and scientific analyses are of paramount importance. Thus, we modified a robust single nucleus dissociation protocol for kidney tissue stored snap frozen or in the preservation media RNA*later* and CellCover. Using porcine kidney tissue as surrogate for human kidney tissue, we conducted single nucleus RNA sequencing with the Chromium 10X Genomics platform. The resulting data sets from each storage condition were analyzed to identify any potential variations in transcriptomic profiles. Furthermore, we assessed the suitability of the preservation media for additional analysis techniques (proteomics, metabolomics) and the preservation of tissue architecture for histopathological examination including immunofluorescence staining. In this study, we show that in daily clinical routines the RNA*later* facilitates the collection of highly preserved kidney biopsies and enables further analysis with cutting-edge techniques like single nucleus RNA sequencing, proteomics, and

histopathological evaluation. Only metabolome analysis is currently restricted to snap frozen tissue. This work will contribute to build tissue biobanks with well-defined cohorts of the respective kidney disease that can be deeply molecularly characterized, opening new horizons for the identification of unique cells, pathways and biomarkers for the prevention, early identification, and targeted therapy of kidney diseases.

Introduction

Independent of the underlying etiology, chronic kidney disease (CKD) constitutes a major risk factor for increased morbidity and mortality as well as progression to end stage kidney disease. Approximately 10% of adults worldwide are affected by CKD and the global burden of chronic kidney disease is growing: CKD is estimated to become the fifth leading cause of death globally by 2040 [1]. In recent decades, scientific effort has shed light on the various pathomechanisms of kidney diseases and the resulting therapies, including renal replacement by dialysis or transplantation. However, most findings are based on model systems (animal and cell models) of the respective kidney disease, limiting the options for targeted therapy and identifying prognostic biomarkers. Therefore, access to high-quality human tissue samples is an important pillar of translational research. The sample quality itself is influenced by various factors such as sample collection, storage, and processing. Biobanks represent an excellent platform for collecting kidney needle biopsies in relevant numbers under standardized conditions, even for rare diseases, and for building well-defined cohorts.

A major challenge for clinically obtained biopsies is the workflow integration into everyday clinical routine, as snap freezing still represents the gold standard for cryopreservation of kidney tissue for certain applications. Human kidney biopsies collected for clinical diagnostics are obtained during the day and often geographically distant from the laboratory, impeding immediate transfer and processing of fresh tissue and snap freezing in liquid nitrogen. A common approach to circumvent these obstacles is to harvest tissue samples for biobanking in cryopreservative agents, such as RNA*later* [2], [3], [4], [5]. RNA*later* is a commercially

81 available, aqueous, nontoxic ammonium sulfate containing tissue storage reagent that
82 preserves instantly the integrity of cellular RNA in tissue samples even at room temperature
83 for up to one week and has shown to be sufficient for long-term protection of cellular RNA at -
84 20°C or -80°C, thus minimizing the need of rapid processing or freezing tissue samples in
85 liquid nitrogen [6], [7], [8]. Recent publications demonstrate that single nucleus dissociation
86 protocols applied to solid tissues such as the kidney stored in RNA*later* at -80°C were suitable
87 for further analyses with single nucleus (sn) RNA sequencing (snRNAseq) protocol [9].
88 However, to the best of our knowledge, neither the possible effects of RNA*later* on the sn
89 transcriptome nor the suitability of RNA*later* stored kidney tissue for proteomics, metabolomics
90 or preservation of kidney tissue architecture and immunofluorescence staining has been
91 examined.
92 The newer formulation CellCover protects DNA, RNA and proteins of cells and solid tissues
93 by instant disruption of cellular degradation pathways immediately after exposure without
94 applying low temperatures. No data exists about storage of CellCover preserved kidney tissue
95 at -80°C for subsequent multi-omic approaches.
96 Single cell (sc) RNAseq was demonstrated to identify unique cells, pathway activity,
97 consecutive targets for novel therapies and preventive and prognostic markers [10], [11], [12],
98 thus supplementing or supporting data derived with other techniques such as bulk RNAseq,
99 proteomics, metabolomics as well as the multiple, complementary types of histological
100 staining. Therefore, a standard for cryopreserving kidney tissue for later deep molecular
101 characterization with multi-omic approaches focusing on snRNseq even months or years after
102 collection is an inevitable step to ensure comparability and reproducibility of data.
103 As human kidney tissue is very valuable and limited, we have used pig kidneys as a surrogate
104 tissue for the studies. Many protocols are optimized for mouse tissue, which is not comparable
105 to healthy and diseased human kidney tissue in terms of fibrotic portions. Pig kidneys, on the
106 other hand, are anatomically very similar to human kidneys, can be easily harvested at local
107 slaughterhouses and no application for animal testing permits is required. Thus, they represent
108 an innovative approach for the development of protocols to reduce the use of laboratory

109 animals, which aligns with the 3Rs principles (replacement, reduction, refinement) in animal
110 research and conserve human tissue.
111

112 Materials and Methods

113 Pig kidney tissue collection and cryopreservation

114 Fresh pig kidneys were obtained from a local slaughterhouse and immediately placed on ice.
115 To mimic clinical settings, the pig kidneys were biopsied with a 16G biopsy needle. The biopsy
116 cores were either immediately frozen in liquid nitrogen or put into 1 ml of RNA*later* (AM7020,
117 Invitrogen) or CellCover (800-050, Anacyte) for 30-60 minutes at 4°C. After incubation, the pig
118 kidney biopsies in RNA*later* and CellCover were placed into a -80°C freezer for at least one
119 month.
120 For immunohistochemical analysis, different freezing conditions were applied to pig kidney
121 biopsies after they incubated for 30-60 minutes in RNA*later* or CellCover at 4°C. They were
122 frozen to -20°C with or without using a CoolCell (479-1840, Corning) and half of the samples
123 were put at -80°C after 7 days. As controls, pig kidney biopsies were embedded in cryomolds
124 (4557, Sakura) with optimal cutting temperature (OCT) medium (4583, Sakura) and frozen in
125 liquid nitrogen. For staining, RNA*later* stored samples were thawed, rinsed with phosphate
126 buffered saline (PBS), formalin-fixed and paraffin-embedded. CellCover stored kidney tissue
127 was thawed and directly paraffin embedded.
128

129 Human kidney tissue

130 For generating snRNAseq data of human kidney tissue, the second core of a clinical indicated
131 allograft needle biopsy and 2 tumor-nephrectomy samples were put in 1ml of RNA*later* for
132 around 60 minutes at 4°C and finally stored at -80°C. Written informed consent was obtained
133 from all individuals and the local ethics committee approved of the studies (PV5026 and
134 PV5822).
135

136 **Kidney tissue dissociation, library preparation and sequencing**

137 **Single nucleus dissociation**

138 A kidney biopsy core was thawed on ice and 3-4 mm of the core were chopped with a razor
139 blade in a petri dish on ice and homogenized using a Dounce homogenizer (D8938-1 SET,
140 Sigma-Aldrich) in 200 µl ice-cold lysis solution and incubated on ice for 20 min with additional
141 3.8 ml of ice-cold lysis solution. If the biopsy core was larger as the 3-4 mm used for single
142 nucleus dissociation, it was put back in RNA*later* and frozen again at -80°C. Lysis solution
143 was prepared with Nuclei PURE lysis buffer (NUC-201, Sigma-Aldrich), 1 mM dithiothreitol
144 (D9779, Sigma-Aldrich) and 0.1 % Triton X-100 (NUC-201, Sigma-Aldrich) according to
145 manufacturer protocol and a RNAse inhibitor mix (0.04 U/µl SUPERaseIN RNAse Inhibitor
146 [AM 2696, Thermo Fisher]; 0.04 U/µl RNAsin Plus RNAse Inhibitor [N2615, Promega]) was
147 added. The single nuclei suspension was filtered through a 30 µm strainer (04-004-2326,
148 Sysmex) and centrifuged at 500g for 5 min at 4°C. The pellet was resuspended and incubated
149 for 2 min in 1ml red blood cell lysis buffer hybri-max™ (R7757-100ml, Sigma Aldrich), filtered
150 through a 5 µm strainer (04-004-2323, Sysmex) and washed with 4 ml of ice cold 0,01% BSA
151 (AM2616, Thermo Fisher) in DPBS (59331C; Sigma) with 0.04 U/µl SUPERaseIN RNAse
152 Inhibitor and 0.04 U/µl RNAsin Plus RNAse Inhibitor at 500 g for 5 min at 4°C. The pellet was
153 resuspended in 1% BSA in DPBS with 0.04 U/µl SUPERaseIN RNAse Inhibitor and 0.04 U/µl
154 RNAsin Plus RNAse Inhibitor.

155

156 **Nuclei loading to the Chromium 10X platform**

157 Nuclei number was counted and samples were diluted prior to loading to the Chromium 10X
158 device to capture ~ 6 000 nuclei of one snap frozen, one RNA*later* and the CellCover stored
159 sample and to capture ~ 10 000 nuclei of two snap frozen and one RNA*later* stored sample
160 The nuclei were separated into Gel Bead Emulsion droplets and libraries were prepared with
161 the Chromium NEXT GEM Single Cell 3' Reagent kits v3.1 according to manufacturer's
162 protocol. The libraries were sequenced on an Illumina Novaseq6000 platform as symmetric

163 paired end run (150 bases) with 200 million raw sequencing reads per sample (pig) or with
164 300 million raw sequencing reads per sample (human). Raw data and count tables for pig can
165 be downloaded from GEO (GSE239442) and for human at Forschungsdatenrepository
166 Hamburg (10.25592/uhhfdm.13026).
167

168 ## Bioinformatics analyses

169 ### Preprocessing and QC

170 10x Genomics raw sequencing data were aligned using the CellRanger software suite
171 (version 6.1.1, 10x Genomics, Pleasanton, CA) including intronic counts. The pig genome
172 Sscrofa11.1 (GCA_000003025.6) was built following the instructions of the 10x Genomics
173 web page for custom genomes using the GTF file (https://www.ensembl.org). The human
174 genome (GRCh38-2020-A) was downloaded from 10x Genomics. Next, SoupX [13] (v1.6.1)
175 was applied with default parameters to remove ambient RNA contamination. Filtering was
176 done by removing cells with < 400 and > 5000 expressed genes. Furthermore, cells with
177 more than 5% mitochondrial expression were excluded. Doublets were removed using
178 Scrublet [14] (default parameters, v0.2.2). Genes, which were expressed in less than 3 cells,
179 were removed.
180

181 ### Dimensionality reduction and clustering

182 After obtaining the sequencing data gene count matrix, subsequent quality control,
183 normalization steps and correction of batch effects (Harmony [15]) provides the basis for a
184 robust downstream analysis. The gene-cell-barcode matrix was log-transformed. PCA was
185 run on the normalized gene-barcode matrix of the top 2000 most variable genes to reduce the
186 number of feature (gene) dimensions. We used Scanpy [16] to perform dimensionality
187 reduction with Uniform Manifold Approximation and Projection (UMAP) to visualize the data
188 and identification of cell populations in combination with the Leiden clustering algorithm
189 (resolution=0.31). The first 20 PCs and 30 neighbors were used for UMAP visualization.

190

191 **Cell type identification based on marker genes and their expression**

192 To identify genes that are enriched in a specific cluster, the mean expression of each gene
193 was calculated across all cells in the cluster. Then each gene from the cluster was compared
194 to the median expression of the same gene from cells in all other clusters. For each cluster,
195 the marker gene list was determined by adjusted p value < 0.05 (sc.rank_genes_groups) and
196 log2FoldChange > 0.5. The highly ranked genes were then used to determine the cell type of
197 each cluster.

198

199 **Proteomic analysis of kidney biopsies**

200 Samples were prepared as previously described with small modifications [17]. In brief, 1-2
201 mm^3 sections of biopsies were washed three times in PBS and then lysed in 8 M urea, 50 mM
202 ammonium bicarbonate, supplemented with 1x Halt protease inhibitor cocktail (Thermo
203 Scientific). Samples were homogenized using glass Dounce homogenizers and then
204 sonicated. Proteins were then precipitated using ice cold acetone to remove any potentially
205 interfering detergents. Protein pellets were re-solubilized in 8M urea, 50 mM ammonium
206 bicarbonate, reduced with 5 mM DTT and alkylated using 10 mM IAA. Overnight digestion was
207 carried out using trypsin at 1:50 enzyme to substrate ratio at 37 °C. Tryptic peptides were
208 acidified to pH 3 using formic acid and purified using in-house made stage-tips [18]. 1 µg of
209 protein was used for LC-MS/MS acquisition.

210 Proteomics data acquisition was carried out on a quadrupole Orbitrap mass spectrometer
211 (QExactive; Thermo Fisher Scientific, Bremen, Germany) coupled to a nano UPLC
212 (nanoAcquity system, Waters) with an inline trap column for desalting and purification
213 (180 µm × 20 mm, 100 Å pore size, 5 µm particle size, Symmetry C18, Waters) followed by a
214 25 cm C18 reversed-phase column for peptide separation (75 µm × 200 mm, 130 Å pore size,
215 1.7 µm particle size, Peptide BEH C18, Waters). Peptides were separated using an 80-minute
216 gradient with linearly increasing ACN concentration from 2% to 30% ACN in 65 minutes using

217 a two-buffer system (buffer A: 0.1% FA in water, buffer B: 0.1% FA in ACN). The mass
218 spectrometer was operated in data-dependent acquisition (DDA) mode with the top 15 ions
219 by intensity per precursor scan (1×10^6 ions, 70,000 Resolution, 240 ms fill time) being
220 selected for MS/MS (HCD at 25 normalized collision energy, 1×10^5 ions, 17,500 Resolution,
221 50 ms fill time) in a range of 400-1200 m/z. A dynamic precursor exclusion of 20 seconds was
222 used. LC-MS/MS data were searched against the UniProt pig reference proteome
223 (downloaded June 2021, 22166 entries) using MaxQuant (version 1.6.3.4) with default
224 parameters. The match between runs (MBR) was disabled, LFQ, IBAQ and classical
225 normalization features were enabled. Data analysis was performed using Perseus software
226 suite (v1.6.15.0) [19]. Missing data was accepted to a threshold of 33% across samples, and
227 missing data were imputed sample wise with a width of 0.3 SD and a downshift of 1.8 SD.
228 Differences were assessed by ANOVA followed by Tukey's HSD.
229 The mass spectrometry proteomics data including FASTA sequences for database searching
230 have been deposited to the ProteomeXchange Consortium via the PRIDE [20] partner
231 repository with the data set identifier PXD044127.
232

233 **Metabolome analysis of cryopreserved pig kidney tissue**

234 Kidney biopsies were grinded in liquid nitrogen before metabolites were extracted as
235 previously [21] described. In brief, metabolites and lipids were simultaneously extracted by
236 adding 1 ml methanol:water (1:1, including internal standards for normalization) and 0.5 ml
237 chloroform (containing internal standard for normalization). The upper phase was subjected
238 to non-targeted metabolomics by gas-chromatography coupled to mass spectrometry (GC-
239 MS), while the lower phase was analyzed by targeted lipid profiling with liquid-chromatography
240 (LC) coupled to multiple-reaction-monitoring (MRM) mass spectrometry. Details about
241 chromatography, mass spectrometry and MRM-transitions can be found in Lagies et al. [21].
242 Data were log-transformed, statistical analysis and visualization were performed by
243 MetaboAnalyst 5.0 [22].

244

245 **Immunofluorescence staining of cryopreserved pig kidney tissue**

246 **De-waxing and antigen retrieval**

247 Paraffin-sections were cut at a thickness of 2-4µm and mounted on SuperFrost plus slides.
248 Then, all samples were sequentially immersed in xylene 3x (10 minutes each) followed by an
249 ethanol series (5 minutes each) of 3x 100%, 2x 70%, 1x 50% and finally 3x (5 minutes each)
250 in double deionized water. Antigen retrieval was performed with Agilent DAKO Target
251 Retrieval Solution pH9 (S236884-2) in a Braun Multiquick FS20 steamer for 15 minutes,
252 followed by a cool-down to room temperature of 30 minutes. The sections were then incubated
253 in Agilent Wash Buffer Solution (K800721-2) for 15 minutes at room temperature.

254

255 **Fluorescent immunolabeling**

256 Samples were incubated with primary antibodies at concentrations according to vendor's
257 guidelines in Agilent Antibody Diluent Solution (CK800621-2) overnight at 4°C, followed by
258 three times washing for 5 minutes with Agilent Wash Buffer Solution. Then, sections were
259 incubated with appropriate secondary antibodies as well as directly conjugated primary
260 antibodies at concentrations according to vendor's guidelines with DAPI (Sigma Aldrich
261 D9542) at a final concentration of 1µg/ml in Agilent Antibody Diluent Solution for 1 hour at
262 room temperature and washed again three times for 5 minutes with Agilent Wash Buffer
263 Solution. All primary antibodies used in this publication are listed in Supplementary Table 1.
264 The following secondary antibodies were used: goat anti-guinea pig Alexa Fluor 555
265 (Invitrogen A21435), goat anti-rabbit Alexa Fluor 647 (Invitrogen A21245). After
266 immunostaining, samples were mounted with ProLong Gold (Invitrogen P36930).

267

268 **Fluorescence imaging of tissues**

269 LED-based widefield imaging of tissues was performed using the THUNDER Imager 3D Live
270 Cell and 3D Cell Culture (Leica Microsystems). Low magnification images were obtained in

271 combination with a 20x objective (NA: 0.40). High magnification images were obtained in
272 combination with a 40x objective (NA: 1.10) after optimizing LED-intensity and exposure times.
273 Fiji imaging software (Max Planck Institute of Molecular Cell Biology and Genetics) was used
274 to navigate the raw files.
275

276 ## Results

277 **Time and tissue saving single nuclei dissociation with standardized lysis buffer**

278 snRNAseq has shown advantages over scRNAseq regarding activation of gene expression
279 artifacts due to warm single cell dissociation protocols, viability, especially of cryopreserved
280 tissue and proportionate cell-type recovery of all major cell types represented in the kidney
281 [23]; [24], [10]. Therefore, we first optimized a single nuclei isolation protocol using a
282 commercially available and thus standardized lysis buffer for cryopreserved kidney tissue that
283 was either snap frozen, stored in RNA*later* or CellCover at -80°C. The pilot studies were
284 performed on needle biopsies of pig kidneys. Furthermore, we reduced filtering and
285 centrifugation steps and performed the entire procedure on ice to minimize gene expression
286 artifacts, as at 4°C the mammalian transcriptional machinery is largely inactive [25].
287 Cryopreservation in RNA*later* and CellCover showed sufficient single nucleus dissociation of
288 pig kidney biopsies after only 25 minutes, while snap frozen pig kidney needed 20 minutes
289 more for a proper dissociation, as examination of nuclei morphology by light microscopy
290 demonstrated (Supplementary Figure 1 A and B). The efficacy of the dissociation protocol was
291 not influenced by the different cryopreservation methods. 3-4 mm of a thawed biopsy core
292 resulted in 300 000-400 000 nuclei independent of the storage condition (data not shown) thus
293 creating the possibility to complement single nucleus sequencing data with data obtained from
294 other analyzing techniques of the same biopsy core. The procedure from thawing the biopsy
295 core to counting and diluting the single nuclei suspension can be completed in approximately
296 60 minutes for immediate processing with any single cell platform.
297

298 **SnRNAseq of cryopreserved pig kidney tissue**

299 Isolated nuclei from each storage condition were further processed with the Chromium 10X
300 platform. Agilent Bioanalyzer traces of cDNA after reverse transcription/amplification and
301 library construction showed the expected fragment size for each cryopreservation condition
302 (Supplemental Figure 1 C, D and E).

303 After sequencing and processing of the Chromium 10X data sets with CellRanger software,
304 the estimated number of cells was on average 9530 nuclei per sample, that was near to the
305 targeted recovery of 10 000. On average, 26 676 total genes and a median number of 2421
306 genes per nucleus were detected. Q30 scores of UMIs, RNA reads and barcodes were mostly
307 above 91.5% (Supplemental Table 2). Counts were normalized such that the total count of
308 each cell was 10,000. The number of detected genes strongly correlated with the total number
309 of RNA reads for snap frozen, RNA*later* and CellCover stored (R^2= 0.94, 0.95, 0.94, Figure 1
310 A). Significant differences in the number of detected genes and the depth of gene expression
311 were observed between RNA*later* and CellCover stored kidney tissue compared to snap
312 frozen kidney tissue ($p< 0.05$, Figure 1 B and C). The total number of RNA reads showed no
313 or only weak correlation with the Mitochondria-associated gene expression for snap frozen,
314 RNA*later* and CellCover preserved samples (R^2=0.15, 0.27 and 0.25, respectively, Figure 2A).
315 However, RNA*later* and CellCover stored samples showed significantly higher fractions of
316 mitochondrial counts ($p< 0.05$, Figure 2B). Besides mitochondrial genes, ambient RNA
317 released during tissue-dissociation can contaminate snRNAseq data sets. It was reported that
318 the highly expressed genes especially from highly abundant cells like the proximal tubule were
319 detected in all cell clusters [11], [23]. Lowest ambient RNA contamination with a fraction of
320 0.055 of all counts was found in RNA*later* compared to snap frozen and CellCover stored
321 kidney tissue (0.066 and 0.086 of all counts, Figure 2C). Nevertheless, the removal of the
322 ambient RNA led to a significant reduction of the number of counts in each condition (Figure
323 2D).

324 After filtering was performed, the recovered number of nuclei was assessed for each storage
325 condition to examine an impact of the storage condition on snRNAseq data quality. Over 90%
326 of the nuclei of data sets from snap frozen, RNA*later* as well as CellCover stored kidney
327 passed the filtering steps and no significant differences between the different cryopreservation
328 methods were observed (Figure 2E). After applying all filtering steps to snRNAseq data sets,
329 31185, 15424 and 6742 nuclei with a median number of 2104, 2645 and 1949 genes/nucleus
330 were recovered in snRNAseq data sets from three snap frozen, two RNA*later* and one
331 CellCover sample stored kidney tissue, respectively.
332
333 **Assessment of preservation-related artifacts in snRNAseq data sets**
334 The quality of the snRNAseq data sets was further evaluated by the ability to define cell types
335 after dimensionality reduction in combination with clustering algorithm (see methods
336 "dimensionality reduction and clustering" for a more detailed description). The six data sets
337 were combined using Harmony [15]. The final combined data set included 53351 nuclei.
338 UMAP analysis revealed that each sample processed with the described protocol contributed
339 to 31 clusters (Figure 3A-C). These clusters showed unique marker gene expression of both
340 common and rare kidney cell types (Fig. 3D-G), including podocytes (POD), 7 populations of
341 endothelial cells (EC, Figure 3F) including glomerular (EC-1, gEC) and lymphatic endothelial
342 cells (EC-7), mesangial cells (MC), fibroblasts (FIB), myofibroblasts (MyoFIB), vascular
343 smooth muscle cells/pericytes (vSMC/P), vascular smooth muscle cells/mesangial cells
344 (vSMC/MC), juxtaglomerular cells (JUXT), interstitial cells (INT), 3 populations of proximal
345 tubules (PT, Figure 3E), tubule cells with markers of proximal tubule cells and podocytes
346 (PODO-PT), thick ascending limb (TAL), distal convoluted tubules (DCT), tubule cells with
347 markers of distal convoluted and connecting tubule cells (DCT/CNT), principal cells (PC),
348 intercalated cells type A and B (IC-A, IC-B), 2 populations of monocytes/macrophages (MAC),
349 t-cells (T-CELL, Figure 3G). No cluster heterogeneity was observed between the different
350 storage conditions (Fig. 3A and C). Proximal tubules showed the highest frequency of all cell

351 types under each cryopreservation condition and the cryopreservation method did not hinder
352 the detection of cells that are present in low proportions in the kidney (Fig.3A and C).
353 A possible impact of RNA*later* and CellCover on the transcriptome of cryopreserved kidneys
354 was intensively evaluated. The mean expressions of the distinct kidney cell types obtained
355 from tissue stored in RNA*later* and CellCover correlated positively with the gold standard snap
356 frozen (R^2=0.82 and 0.75, Figure 4A). To gain further insights into cell-specific preservation-
357 related artifacts, we compared the differential gene expression of each cell-type of RNA*later*
358 or CellCover stored kidney tissue separately with that of snap frozen tissue. In RNA*later* and
359 CellCover stored samples, 24 and 24 cell types, respectively, showed significant upregulation,
360 while 25 and 29 cell types, respectively, had a down regulated gene expression ($p < 0.05$)
361 when compared to snRNAseq data sets from snap frozen kidney tissue (Figure 4B).
362 Glomerular cells like podocytes, glomerular endothelial cells and mesangial cells represent
363 rare kidney cell types, which are often enriched for scientific purposes as primary cell cultures
364 or from abundant experimental tissue. Transcriptional changes that might be induced by
365 RNA*later* or CellCover would significantly reduce data quality. To rule out transcriptional
366 differences of glomerular cells between single nucleus data sets obtained from kidneys stored
367 in RNAl*ater*, CellCover or snap frozen, we calculated the receiver operator characteristic curve
368 (AUROC) score. using MetaNeighbor [26]. Each glomerular cell type obtained from the
369 respective storage condition had a very high AUROC score for the corresponding cell type
370 obtained from one of the other two storage conditions (Figure 4C), indicating high similarity of
371 cell types obtained by the different storage conditions.
372 Snap frozen kidney needle biopsies are immediately frozen after collection, allowing less time
373 for the induction of transcriptional changes due to alterations in cellular homeostasis. RNA*later*
374 and CellCover facilitate the handling of kidney biopsies because they can be frozen later. To
375 investigate whether delayed freezing induces cellular stress responses, response to hypoxia
376 or apoptosis, we conducted an enrichment analysis of these pathways with AUCell [27].
377 In all cell types of the kidney biopsies stored in RNAlater, CellCover or snap frozen we
378 detected a similar activation of the stress response pathways (Figure 4D). Additionally, we

379 found no differences in the expression of genes related to the hypoxia and apoptosis signaling
380 in most cell types under any of the storage conditions tested (Figure 4D). The expression
381 levels of the canonical stress response genes *HSP90AB1*, *HSPB1*, *HSPA8*, *HSPA5*,
382 *HSP90B1* and *DNAJA1* were moderate, and we observed low expression levels of the
383 apoptosis markers *PPP1R15A*, *ATF3*, *DYNLL1*, *LER3*, *LMNA*, *UBC*, *UBB*, *JUNB*, *TPT1*, *FOS*,
384 *FOSB* and *EGR1* in all storage conditions (Figure 4E).
385 Overall, the single nuclear transcriptome of RNAlater, CellCover or snap frozen stored kidney
386 tissue did not substantially differ, but kidney tissue stored in RNA*later* showed slightly smaller
387 differences in quality control metrics than tissue stored in CellCover compared to snap frozen
388 tissue.
389

390 **Single nucleus analysis of healthy and diseased human kidney biopsies**

391 To confirm that porcine kidney tissue constitutes a suitable surrogate for human kidney tissue,
392 fractions from a human kidney allograft biopsy and healthy kidney tissue of 2 tumor-
393 nephrectomies stored in RNA*later* at -80°C were subjected to the snRNAseq pipeline we
394 established with pig kidney tissue. After sequencing and processing the data sets with
395 CellRanger software, the analysis revealed an average estimated number of 15944 nuclei per
396 tumor-nephrectomy sample and a median number of 943.5 genes per nucleus were detected
397 in the tumor-nephrectomy samples. The data set obtained from the diseased kidney biopsy
398 yielded an estimated number of 11313 nuclei and a median number of 2057 genes per nucleus
399 (Supplementary Table 3). After filtering with the described parameter, dimensionality reduction
400 and integration of the 3 data sets with Harmony [15] (Figure 5A), a total number of 43010
401 nuclei clustered into the diverse cell types of the kidney (Figure 5B) that were annotated on
402 the basis of the expression patterns of cell-specific marker genes reported for previous kidney
403 single-cell data sets (Figure 5C) [10], [28].
404

405 **Proteomics of cryopreserved pig kidney tissue**

406 Next, we sought to determine the suitability of RNA*later* and CellCover stored kidney tissue
407 for proteome-analysis by using mass spectrometry. The proteome-analysis of snap frozen,
408 RNA*later* and CellCover stored pig kidney tissue resulted in a complete data set of 1670
409 proteins (Supplementary Table 4). Globally, the detected protein LFQ intensity across
410 conditions and replicates was consistent (Figure 6A).
411 Principal component analysis between the different cryopreservation methods showed high
412 similarity between tissue stored in RNA*later* compared to snap frozen tissue (Figure 6B), with
413 principal component (PC) 1 being very similar and PC2 playing a smaller contribution to the
414 observed difference (13,92% PC2 vs 39,14% PC1). The proteome of CellCover stored kidney
415 tissue was markedly different along PC1 and somewhat different along PC2 compared to snap
416 frozen tissue. In contrast to RNA*later*, our proteomic analysis indicates that 659 of 1670
417 proteins had a different abundance when comparing CellCover and snap frozen tissue
418 (adjusted p-value <0.05, Supplementary Table 4).
419 We further aimed to investigate possible cell type specific differences between RNA*later*,
420 CellCover and snap frozen stored kidney tissue in the proteome. The 20 most upregulated
421 genes for each cell type were extracted and used to compute module scores in the proteome.
422 Two cell type specific differences were found in RNA*later* stored kidney tissue compared to
423 snap frozen tissue, whereas 18 of 31 cell types obtained from CellCover stored tissue showed
424 significant differences in the proteome compared to snap frozen tissue (Figure 6C). In this
425 study we can show that proteome analysis of RNA*later* provides comparable results to snap
426 frozen kidney tissue. Proteome analysis of CellCover stored kidney tissue revealed lower
427 concordance to snap frozen tissue, more than 39% of the proteins had different abundances.
428

429 **Metabolomics of cryopreserved pig kidney tissue**

430 In metabolomics, LC-MS and GC-MS are two complementary, commonly used techniques.
431 Metabolites must be volatile or otherwise must be derivatized prior to GC-MS analysis, which
432 limits the compounds suitable for this technique. However, GC-MS delivers excellent

433 chromatographic separation, and its ionization mechanism covers a wide range of compound
434 classes. LC-MS is not as limited as GC-MS regarding analyte properties, harbors good
435 chromatographic separation, but its ionization technique is not as universal as in GC-MS.
436 Thus, we used a combination of targeted LC-MS and non-targeted GC-MS to study the
437 influence of cryo-preservation reagents on the renal metabolome.
438 In our study, data from non-targeted GC-MS analysis could not be used since small molecules
439 introduced by the two cryoconservation reagents strongly suppressed the signals derived from
440 metabolites. These conservation reagents might also interfere with the derivatization reaction
441 required for GC-MS analyses. In fact, the intensities of the internal standards in the RNA*later*
442 samples decreased to approximately 50% of the snap frozen condition and many metabolites
443 present in the snap frozen samples were not detected at all in either conserved condition.
444 Next, the lipophilic extracts were analyzed by targeted lipid profiling. Mass spectrometric
445 analysis was possible, probably since the conservation reagents and buffer salts remained in
446 the aqueous phase. As shown in the PC analysis, snap frozen control tissue was clearly
447 different from both tested conservation methods (Figure 7A). Remarkably, CellCover's
448 variance was responsible for most observed alterations, as it scattered around PC1. RNA*later*
449 also exhibited a much higher variation than snap frozen tissue. This is reflected in the averages
450 of the coefficients of variation with 0.07 in the quality control sample, 0.20 in the snap frozen
451 tissue samples, 0.51 in RNA*later* and even 0.62 in CellCover.
452 A comparison of lipids altered between RNA*later* and snap frozen revealed several enriched
453 free fatty acids and lyso-phospholipids (Figure 7B). A very similar pattern was observed in
454 samples preserved in Cell Cover (Figure 7C). In the latter comparison, several lipids were
455 enriched more than fourfold compared to snap frozen, but only had a p-value < 0.1. All these
456 lipids were again free fatty acids and lyso-phospholipids. The p-values might be explained by
457 the high variance in this group. A specific accumulation of these two lipid classes indicates an
458 insufficient metabolic quenching by still active lipases. While snap frozen kidney tissue is
459 suitable for metabolomics with current technologies, RNA*later* and CellCover stored kidney
460 are not.

461

462 **Histopathological evaluation of tissue architecture and antigenicity of**

463 **cryopreserved pig kidney tissue**

464 To address whether RNA*later* and CellCover preserve kidney tissue structural architecture
465 and molecular antigenicity, conventional histopathological with periodic acid-Schiff (PAS)and
466 immunofluorescence (IF-) staining from pig kidney stored in RNA*later* and CellCover were
467 performed and compared to OCT-embedded tissue as control.

468 To determine the optimal storage conditions, pig kidney tissue stored in RNA*later* and
469 CellCover were either placed immediately in -20°C after an initial short incubation at 4°C for
470 30 to 60 minutes or underwent an automated, controlled cool-down at a rate of −1°C/minute
471 to -20°C. RNA*later* embedded kidney tissue was well preserved at -20°C, independent of
472 immediate (Figure 8A) or automated, controlled (Supplementary Figure 2) freezing condition.
473 CellCover preserved kidney tissue appeared to be less well preserved compared to RNA*later*
474 embedded tissue, as a higher proportion of cells were detached from the basement membrane
475 (Figure 8B). No difference in IF-staining signal quality was observed between RNA*later* and
476 CellCover preserved kidney tissues (Figure 8C and D).
477 Structural architecture and molecular antigenicity of RNA*later* and CellCover preserved kidney
478 tissue was additionally examined after freezing from -20°C to -80°C for long time storage.

479 Freezing of RNA*later* and CellCover preserved kidney tissue from -20°C to -80°C did not
480 introduce more freezing-related artifacts (Figure 8E and F) as freezing to -20°C only or as
481 OCT-embedding (Figure 8G). Again, we found that kidney tissue frozen in CellCover appeared
482 to be less well preserved compared to RNA*later* preserved tissue. Similarly, molecular
483 antigenicity was preserved in both RNA*later* and CellCover embedded kidney tissues that
484 underwent freezing from -20°C to -80°C as shown by IF-staining (Figure 8H and I) and yielded
485 comparable results to OCT-embedded kidney control-tissue (Figure 8J).

486 Overall, this study could demonstrate that both RNA*later* and CellCover preserve kidney tissue
487 molecular antigenicity at -80°C. However, the structural architecture appeared to be more
488 intact in RNAlater stored tissue.
489

490 ## Discussion

491 Single cell transcriptomic studies contributed to substantial progress in understanding kidney
492 tissue heterogeneity and provided greater insight into the complex cell type composition and
493 orchestrated signaling pathways in healthy and diseased tissue [10], [11], [23]. This technique
494 opens doorways for the identification of targeted therapy and prognostic biomarkers. However,
495 kidney tissue stored in biobanks is cryopreserved and therefore, depending on the
496 preservation method, usually not suitable for scRNAseq since these methods require intact
497 viable single cells. DMSO-containing cryopreservation media, which maintain cell viability
498 during freezing, storage and thawing require liquid nitrogen for storage [30], [31], that mostly
499 limits storage capacities of biobanks. Published single nucleus dissociation protocols have
500 demonstrated substantial advantages including greater flexibility with time and place of
501 analysis, the representation of rare and fragile kidney cell types, reduction of dissociation
502 induced transcriptional stress responses and comparable sensitivity to scRNAseq [10], [23].
503 These findings are crucial for ushering in a new era of translational research, as single cell
504 analyses are no longer limited to mainly experimental tissue. One hurdle still to be overcome
505 is the collection of high-quality kidney tissue for biobanks, which should be translatable into
506 clinical practice. Although comprehensive studies examined the advantages of single nucleus
507 over single cell dissociation and highlighted the compatibility of archived frozen tissue [23],
508 [32], [33], an evaluation of a potential kidney cell-type specific transcriptional impact of
509 preservation media such as RNA*later* or CellCover, which facilitate tissue collection for
510 repositories in daily clinical practice, has been lacking.-Thus, we optimized a tissue processing
511 pipeline for kidney biopsies stored in RNA*later*, that allows snRNAseq, proteome and
512 histopathological analysis.

513 First, we demonstrated that our adapted robust single nucleus dissociation protocol for 3-4
514 mm of snap frozen or RNA*later* and CellCover stored kidney biopsy cores yielded in sufficient
515 numbers of intact nuclei for further processing with the high throughput single cell platform
516 Chromium 10X Genomics. High throughput technologies permit the analysis of thousands of
517 cells in parallel if enough high-quality single cells/nuclei can be provided. Especially when
518 investigating less abundant cell populations like glomerular cells, the total number of profiled
519 cells is crucial [34].
520 Sequencing quality control metrics revealed significantly lower fractions of ambient RNA but
521 higher mitochondrial contamination in snRNAseq data sets obtained from RNA*later* stored
522 kidney tissue compared to snap frozen tissue. In snRNAseq data sets from CellCover stored
523 tissue, both mitochondrial and ambient RNA contamination was found to be significantly higher
524 as in snap frozen snRNAseq data sets. Although mitochondrial transcripts are not expressed
525 in the nucleus, they were reported to be present in variable quantities in snRNAseq data sets
526 due to association with the nuclear membrane [10]. Elevated mitochondrial transcript are
527 indicators for cell stress [35], but enrichment analysis of the single nuclear transcriptome of
528 snap frozen, RNA*later* and CellCover stored kidney tissue did not uncover relevant differences
529 in apoptosis, hypoxia and cellular response to stress pathways. Two possible causes can
530 underlie these controversial findings. First, RN*Alater* and CellCover could increase
531 mitochondrial adhesion to the nuclear membrane. The preservation media might alter
532 membrane surfaces which could also explain the finding of slightly increased multiplets in
533 RNA*later* and CellCover preserved samples compared to snap frozen. Second, each data set
534 was generated from an individual (sacrificed) pig with possibly interindividual varying
535 mitochondrial abundance. However, our data sets show a low overall mitochondrial transcripts
536 abundance of < 2.5% and do not exceed previous reported numbers of mitochondrial
537 contamination [10], [9], [10].
538 Applying all filter criteria to the snRNAseq data sets, the number of recovered nuclei exceeded
539 previously published results for snap frozen [36] and RNA*later* stored kidney tissue [9].

540 Depending on the underlying kidney disease, cell type specific transcriptional changes
541 induced by RNA*later* or CellCover might lead to misinterpretation of results for disease
542 mechanisms, potential targets, and biomarkers. Thus, we performed cell type specific
543 differential expression analysis between RNA*later* or CellCover and snap frozen stored kidney
544 tissue. Up-regulation of genes was overall low in both preservation methods, CellCover
545 showed somewhat more downregulated genes over all cell types. This finding might be
546 attributed to preservation medium specific transcriptional changes or interindividual
547 differences of the respective pig kidneys.
548 As fractions of kidney biopsies provide limited numbers of glomeruli and glomerular cells
549 represent lower proportions of the kidney [34] transcriptional programs altered by RNA*later* or
550 CellCover will have higher impact as in abundant cell types. We could not detect any influence
551 of the storage condition of the single nuclear transcriptome of 3 glomerular cell types
552 (podocytes, glomerular endothelial cells, mesangial cells).
553 In contrast to previous studies, which commonly reported a lower detection rate of immune
554 cells in snRNAseq data sets compared to scRNAseq data sets [37], [10], [23], [38] our protocol
555 was able to recover a total of 1896 immune cells in the data sets of pig kidney, clustering into
556 t-cells and monocytes/macrophages. To minimize the loss of rare cell types such as immune
557 cells, the entire protocol was performed on ice, the number of sieving and centrifugation steps
558 was reduced, and a harsh lysis buffer shortened the dissociation time by rapidly releasing
559 even strong cellular associations. Incomplete cell dissociation in scRNAseq protocols might
560 lead to under-representation of resident cell types and artificially increases leukocyte rates in
561 the tissue [38].
562 We further demonstrated that porcine kidney tissue represents a surrogate for human kidney
563 tissue, as we were able to apply our protocol without any modification to 1 human diseased
564 kidney biopsy and 2 healthy controls (tumor-free tissue from tumor-nephrectomies). These
565 findings are consistent with previously published results for heart tissue [33].
566 Overall, our rigorous snRNAseq data analysis of RNA*later* stored kidney tissue could outline
567 that RNA*later* constitutes an adequate alternative for immediate tissue preservation if snap

568 freezing of tissue is not implementable into clinical routines. In addition to slightly higher
569 concordance of quality control metrics of snRNAseq data sets from RNAlater and snap frozen
570 kidney tissue, a major advantage of RNAlater over CellCover is its long-time experience in
571 tissue RNA protection [6], [39].
572 As our optimized protocol requires only 3-4 mm of a biopsy core for high throughput
573 snRNAseq, the remaining part of a biopsy core stored in RNA*later* or CellCover can be utilized
574 to generate other omics data. Tissue stored in RNA*later* can be refrozen in contrast to
575 CellCover and snap frozen tissue, therefore further analysis techniques are independent of
576 time and place. Although samples stored in RNA*later* have been used extensively in DNA and
577 RNA studies, only a few studies have investigated the feasibility in retrieving proteins,
578 metabolites or histopathological information from human tissue samples stored in RNA*later*
579 [40], [41], [2], [3].
580 The investigation of one kidney biopsy core stored in RNA*later* with additional data dimensions
581 by combining single cell resolution of transcriptome data with bulk data of intra- and
582 extracellular proteins as well as spatial resolution of imaging [42] will be a major step in
583 translational medicine and overcome the need of disease model systems. In addition, the
584 generation of these data sets provides the basis for the need to develop novel bioinformatics
585 and mathematical modeling tools and represents a further step towards personalized
586 medicine, as Riedel et al. were already able to demonstrate glucocorticoid response in patients
587 with crescentic glomerulonephritis by analyzing histological and single cell data obtained
588 directly from fresh kidney biopsies [43]. As previously reported for tumor tissue of pancreatic
589 ductal adenocarcinoma [41], we could demonstrate that mass spectrometry proteome analysis
590 of RNA*later* stored kidney tissue matched highly with snap frozen kidney tissue and no protein
591 showed a significant difference between both storage conditions.
592 In addition, we computationally generated cell type-specific modules with sn RNAseq data
593 sets and compared these modules in the proteomic data between the three storing conditions.
594 The cell type specific modules from RNA*later* stored kidney showed comparable protein
595 abundance to those from snap frozen tissue. More differences were detected in CellCover

596 stored kidney tissue. For proteome analysis, only one pig kidney was preserved by the
597 different preservation methods, thus the differences found for CellCover stored tissue can be
598 attributed to the medium.
599 The metabolome is relevant for understanding of physiological and disease-modifying
600 mechanisms as well as its interaction with the transcriptome and proteome of the kidney is
601 only beginning to be understood [44]. However, this study illustrates that with current
602 technologies only snap frozen kidney biopsies can be used for metabolomics studies.
603 Preservation of kidney tissue architecture is essential for bio banked tissue, as morphologic
604 examination of kidney tissue biopsies is still essential for histopathological diagnosis. In
605 addition, preserved architecture of archived tissue might constitute added value not only for
606 scientific efforts, but also for ethical aspects of kidney tissue biobanks. Kidney tissue stored in
607 RNA*later* could be used as supplemental material if the kidney tissue collected for clinical
608 histopathology does not contain enough informative material and would otherwise require a
609 new invasive procedure for a definitive diagnosis of the underlying kidney disease.
610 Moreover, disease-specific morphological and molecular alterations can be assessed by
611 artificial intelligence (AI) -driven pattern extraction and improve disease classifications,
612 pathogenesis and prognosis as well as therapy response [45], [46]. AI-defined morphological
613 and molecular patterns can be integrated with data obtained from other, complementary omics
614 like sn transcriptomics and proteomics. In our study we show that RNA*later* mostly preserves
615 kidney architecture and does not interfere with immunofluorescence staining. We tested PAS
616 and a limited number of antibodies for immunofluorescence staining of RNA*later* preserved
617 porcine kidney tissue. In contrast to our study, a previous study demonstrated impaired
618 histological structure and immunohistochemical staining patterns for mouse kidneys stored in
619 RNA*later* at -20°C. These contrasting results may be explained by a longer incubation time of
620 the mouse tissue at 4°C overnight prior to freezing to -20°C [47]. CellCover stored kidney
621 tissue was less suitable for histopathological examination in our hands.
622 However, our study has several limitations that require further investigation. First, additional
623 studies with a larger number of antigens and with different types of imaging on human tissues

624 are needed to further evaluate the preservation of tissue morphology and the protein-
625 preserving effect of *RNA*later. Second, we did not investigate whether or how the duration of
626 tissue cryopreservation and long-term storage affects the dissociation and integrity of cell
627 nuclei, the single-cell transcriptome landscape or proteome, and the structural architecture
628 and molecular antigenicity of kidney tissue. Finally, we did not examine the transcriptomic
629 landscape of single cells between fresh and cryopreserved tissue preparations.
630 In conclusion, our study shows that RNA*later* can facilitate the collection and storage of kidney
631 tissue by bypassing the need for snap freezing in liquid nitrogen without compromising
632 snRNAseq, proteome and histopathological analysis. Only metabolome analysis is currently
633 limited to snap frozen stored kidney biopsies.
634 This work will guide future efforts to illuminate the molecular landscape of kidney diseases by
635 applying multi-omic approaches to translational medicine, enabled by the integration of tissue
636 collection for biobanking into clinical routines.
637

638 ## Authors Contributions

639

640 S.E.G., S.H. and M.T.L. conceptualized, designed, conducted, and interpreted experiments
641 and analyses. R.K., F.H. and S.H. designed and conducted the bioinformatic analyses. M. P.
642 and T.Z. assisted with data handling. D.K, S.L., M.La., B.K. conceived and analyzed
643 experiments. S.Lu and S.Liu provided input in experimental design and assisted with data
644 interpretation. S.C. and I.E. performed experiments. J.C. provided critical samples.
645 F.B., V.G.P., M.M.R., T.B.H and S.B. gave input in experimental design and provided critical
646 review and commentary. S.E.G, S.H., M.T.L. and T.B.H. supervised the project. S.E.G., S.H.,
647 M.T.L, and T.B.H. wrote the manuscript with input and discussion from all authors.
648

649 ## Acknowledgements

650 The authors acknowledge excellent technical support by Stefan Gatzemeier. R.K. was
651 supported by FOR5068 P9 and the 3R initiative of the UKE; F.H. by the M3I excellence
652 initiative and a UKE postdoctoral stipend; and S.B. by SFB1286 SP02, SFB1192 B8, and C3.
653 S.H. was supported by SFB1192 B8. F.B. was supported by the Else Kröner-Fresenius-
654 Stiftung (2021_EKMS.26) and the German Society of Nephrology. D.K. received intramural
655 funding (Clinician/Scientist program). M.M.R was supported by the DFG (RI 2811/1-1 and RI
656 2811/2-1, FOR2743, and SFB1192-project B10), by the Young Investigator Award from the
657 Novo Nordisk Foundation, grant number NNF19OC0056043, the Carlsberg Young
658 Investigator fellowship as well as Aarhus universitet forskningsfond, and an endowed
659 professorship by the Klinikum Bad Bramstedt. M.M.R. thanks the Klinikum Bad Bramstedt for
660 support. This project was also supported by the European Union's Horizon 2020 research and
661 innovation funding programme under the Marie Skłodowska-Curie grant agreement No
662 754513 and The Aarhus University Research Foundation (to M.M.R). M.T.L was supported by
663 BMBF, grant 01GM1518A; STOP-FSGS and BMBF grant 01EK2105D, UPTAKE. T.B.H was
664 supported by the DFG (CRC1192, HU 1016/8–2, HU 1016/ 12–1), by the BMBF (STOP-
665 FSGS- 01GM1901C, UPTAKE 01EK2105D). This project has received funding from Abbvie
666 and the Innovative Medicines Initiative 2 Joint undertaking under grant agreement No. 115974
667 (Beat-DKD) (to T.B.H). This Joint undertaking receives support from the European Union's
668 Horizon 2020 research and innovation program and EFPIA with JDRF. This work was partially
669 funded by the Else Kröner-Fresenius-Stiftung and the Eva Luise und Horst Köhler Stiftung –
670 Project No: 2019_KollegSE.04 (to S.G. and T.B.H).

671 **References**

672 1. Kovesdy, C.P., *Epidemiology of chronic kidney disease: an update 2022.* Kidney Int
673 Suppl (2011), 2022. **12**(1): p. 7-11.

674 2. Lindner, M., et al., *Quality assessment of tissue samples stored in a specialized*
675 *human lung biobank.* PLOS ONE, 2019. **14**(4): p. e0203977.

676 3. Ellis, M., et al., *Development and validation of a method for using breast core needle*
677 *biopsies for gene expression microarray analyses.* Clin Cancer Res, 2002. **8**(5): p.
678 1155-66.

679 4. Dekairelle, A.-F., et al., *Preservation of RNA for functional analysis of separated*
680 *alleles in yeast: comparison of snap-frozen and RNALater® solid tissue storage*
681 *methods.* 2007.

682 5. Guo, D. and D.R. Catchpoole, *Isolation of intact RNA following cryosection of*
683 *archived frozen tissue.* Biotechniques, 2003. **34**(1): p. 48-50.

684 6. Cohen, C.D., et al., *Quantitative gene expression analysis in renal biopsies: a novel*
685 *protocol for a high-throughput multicenter application.* Kidney Int, 2002. **61**(1): p. 133-
686 40.

687 7. Mutter, G.L., et al., *Comparison of frozen and RNALater solid tissue storage methods*
688 *for use in RNA expression microarrays.* BMC Genomics, 2004. **5**: p. 88.

689 8. Wolfe, L.M., et al., *Banking placental tissue: an optimized collection procedure for*
690 *genome-wide analysis of nucleic acids.* Placenta, 2014. **35**(8): p. 645-54.

691 9. Rousselle, T.V., et al., *An optimized protocol for single nuclei isolation from clinical*
692 *biopsies for RNA-seq.* Sci Rep, 2022. **12**(1): p. 9851.

693 10. Lake, B.B., et al., *A single-nucleus RNA-sequencing pipeline to decipher the*
694 *molecular anatomy and pathophysiology of human kidneys.* Nat Commun, 2019.
695 **10**(1): p. 2832.

696 11. Park, J., et al., *Single-cell transcriptomics of the mouse kidney reveals potential*
697 *cellular targets of kidney disease.* Science, 2018. **360**(6390): p. 758-763.

698 12. Young, M.D., et al., *Single-cell transcriptomes from human kidneys reveal the cellular*
699 *identity of renal tumors.* Science, 2018. **361**(6402): p. 594-599.

700 13. Young, M.D. and S. Behjati, *SoupX removes ambient RNA contamination from*
701 *droplet-based single-cell RNA sequencing data.* Gigascience, 2020. **9**(12).

702 14. Wolock, S.L., R. Lopez, and A.M. Klein, *Scrublet: Computational Identification of Cell*
703 *Doublets in Single-Cell Transcriptomic Data.* Cell Syst, 2019. **8**(4): p. 281-291.e9.

704 15. Korsunsky, I., et al., *Fast, sensitive and accurate integration of single-cell data with*
705 *Harmony.* Nat Methods, 2019. **16**(12): p. 1289-1296.

706 16. Wolf, F.A., P. Angerer, and F.J. Theis, *SCANPY: large-scale single-cell gene*
707 *expression data analysis.* Genome Biol, 2018. **19**(1): p. 15.

708 17. Rinschen, M.M., et al., *Quantitative deep mapping of the cultured podocyte proteome*
709 *uncovers shifts in proteostatic mechanisms during differentiation.* Am J Physiol Cell
710 Physiol, 2016. **311**(3): p. C404-17.

711 18. Rappsilber, J., Y. Ishihama, and M. Mann, *Stop and go extraction tips for matrix-*
712 *assisted laser desorption/ionization, nanoelectrospray, and LC/MS sample*
713 *pretreatment in proteomics.* Anal Chem, 2003. **75**(3): p. 663-70.

714 19. Tyanova, S., et al., *The Perseus computational platform for comprehensive analysis*
715 *of (prote)omics data.* Nat Methods, 2016. **13**(9): p. 731-40.

716 20. Perez-Riverol, Y., et al., *The PRIDE database resources in 2022: a hub for mass*
717 *spectrometry-based proteomics evidences.* Nucleic Acids Res, 2022. **50**(D1): p.
718 D543-d552.

719 21. Lagies, S., et al., *Metabolic and Lipidomic Assessment of Kidney Cells Exposed to*
720 *Nephrotoxic Vancomycin Dosages.* Int J Mol Sci, 2021. **22**(18).

721 22. Pang, Z., et al., *MetaboAnalyst 5.0: narrowing the gap between raw spectra and*
722 *functional insights.* Nucleic Acids Res, 2021. **49**(W1): p. W388-w396.

723 23. Wu, H., et al., *Advantages of Single-Nucleus over Single-Cell RNA Sequencing of*
724 *Adult Kidney: Rare Cell Types and Novel Cell States Revealed in Fibrosis.* J Am Soc
725 Nephrol, 2019. **30**(1): p. 23-32.

726 24. Lacar, B., et al., *Nuclear RNA-seq of single neurons reveals molecular signatures of*
727 *activation.* Nat Commun, 2016. **7**: p. 11022.

728 25. Adam, M., A.S. Potter, and S.S. Potter, *Psychrophilic proteases dramatically reduce*
729 *single-cell RNA-seq artifacts: a molecular atlas of kidney development.* Development,
730 2017. **144**(19): p. 3625-3632.

731 26. Crow, M., et al., *Characterizing the replicability of cell types defined by single cell*
732 *RNA-sequencing data using MetaNeighbor.* Nat Commun, 2018. **9**(1): p. 884.

733 27. Aibar, S., et al., *SCENIC: single-cell regulatory network inference and clustering.* Nat
734 Methods, 2017. **14**(11): p. 1083-1086.

735 28. Hansen, J., et al., *A reference tissue atlas for the human kidney.* Sci Adv, 2022.
736 **8**(23): p. eabn4965.

737 29. Garcia, A. and C. Barbas, *Gas Chromatography-Mass Spectrometry (GC-MS)-Based*
738 *Metabolomics*, in *Metabolic Profiling: Methods and Protocols*, T.O. Metz, Editor.
739 2011, Humana Press: Totowa, NJ. p. 191-204.

740 30. McRae, A., et al., *A Protocol for the Cryopreservation of Human Intestinal Mucosal*
741 *Biopsies Compatible With Single-Cell Transcriptomics and Ex Vivo Studies.* Front
742 Physiol, 2022. **13**: p. 878389.

743 31. Arazi, A., et al., *The immune cell landscape in kidneys of patients with lupus*
744 *nephritis.* Nat Immunol, 2019. **20**(7): p. 902-914.

745 32. Habib, N., et al., *Massively parallel single-nucleus RNA-seq with DroNc-seq.* Nat
746 Methods, 2017. **14**(10): p. 955-958.

747 33. Pimpalwar, N., et al., *Methods for isolation and transcriptional profiling of individual*
748 *cells from the human heart.* Heliyon, 2020. **6**(12): p. e05810.

749 34. Deleersnijder, D., et al., *Current Methodological Challenges of Single-Cell and*
750 *Single-Nucleus RNA-Sequencing in Glomerular Diseases.* J Am Soc Nephrol, 2021.
751 **32**(8): p. 1838-1852.

752 35. Osorio, D. and J.J. Cai, *Systematic determination of the mitochondrial proportion in*
753 *human and mice tissues for single-cell RNA-sequencing data quality control.*
754 Bioinformatics, 2021. **37**(7): p. 963-967.

755 36. Wilson, P.C., et al., *The single-cell transcriptomic landscape of early human diabetic*
756 *nephropathy.* Proc Natl Acad Sci U S A, 2019. **116**(39): p. 19619-19625.

757 37. Wu, H., et al., *Single-Cell Transcriptomics of a Human Kidney Allograft Biopsy*
758 *Specimen Defines a Diverse Inflammatory Response.* J Am Soc Nephrol, 2018.
759 **29**(8): p. 2069-2080.

760 38. Denisenko, E., et al., *Systematic assessment of tissue dissociation and storage*
761 *biases in single-cell and single-nucleus RNA-seq workflows.* Genome Biol, 2020.
762 **21**(1): p. 130.

763 39. Mariani, L.H., et al., *Precision nephrology identified tumor necrosis factor activation*
764 *variability in minimal change disease and focal segmental glomerulosclerosis.* Kidney
765 Int, 2023. **103**(3): p. 565-579.

766 40. Bennike, T.B., et al., *Comparing the proteome of snap frozen, RNAlater preserved,*
767 *and formalin-fixed paraffin-embedded human tissue samples.* EuPA Open Proteom,
768 2016. **10**: p. 9-18.

769 41. Bae, J., et al., *Comprehensive proteome and phosphoproteome profiling shows*
770 *negligible influence of RNAlater on protein abundance and phosphorylation.* Clin
771 Proteomics, 2019. **16**: p. 18.

772 42. Rinschen, M.M. and J. Saez-Rodriguez, *The tissue proteome in the multi-omic*
773 *landscape of kidney disease.* Nat Rev Nephrol, 2021. **17**(3): p. 205-219.

774 43. Riedel, J.H., et al., *Glucocorticoids target the CXCL9/CXCL10-CXCR3 axis and*
775 *confer protection against immune-mediated kidney injury.* JCI Insight, 2023. **8**(1).

776 44. Rinschen, M.M., et al., *Metabolic rewiring of the hypertensive kidney.* Sci Signal,
777 2019. **12**(611).

778 45. Becker, J.U., et al., *Artificial intelligence and machine learning in nephropathology.*
779 Kidney Int, 2020. **98**(1): p. 65-75.

780 46. Zimmermann, M., et al., *Deep learning-based molecular morphometrics for kidney*
781 *biopsies.* JCI Insight, 2021. **6**(7).

782 47. Suhovskih, A.V., et al., *Suitability of RNALater solution as a tissue-preserving*
783 *reagent for immunohistochemical analysis.* Histochem Cell Biol, 2019. **152**(3): p. 239-
784 247.

785

786 ## Figure Legends:

787 **Fig. 1:** Scatter plot representation depicting the relationship of the number of detected genes (y-axis)
788 against the total number of RNA reads (x-axis) for snap frozen (R^2= 0.94), RNA*later* (R^20= 0.94) and
789 CellCover (R^2=0.95) stored kidney tissue (A). Comparison of the sequencing quality metrics total
790 number of RNA reads (B) and total number of genes (C) between snRNAseq data sets obtained from

791 different cryopreservation methods (snap frozen, RNAlater and CellCover stored kidney tissue). ****= p
792 < 0.05

793 **Fig. 2**.: Comparison of quality metrics of 6 snRNAseq data sets from 3 snap frozen, 2 RNAlater and 1
794 CellCover cryopreserved pig kidney biopsies. (A) Correlation of the total number of molecules detected
795 within a nucleus with percentage of mitochondria present in each cell averaged for each method. (B)
796 Distribution of percentage of mitochondria in each cell per method. (C) Distribution of the ratio of
797 ambient RNA and total RNA as reported by SoupX. (D) Distributions of nuclei containing ambient RNA
798 and after removal with SoupX. The counts are log transformed for better visualization. (E) Number of
799 remaining nuclei after each filtering step, including scrublet for multiplet removal, removal of nuclei with
800 < 400 genes (min genes), removal of nuclei with > 5% mitochondrial counts (pct mito) and removal of
801 nuclei with > 5000 genes (max genes). ****= p<0.05

802 **Fig. 3**: UMAP visualization of a total of 53.351 nuclei from a total of 6 pig kidneys after quality control
803 filtering. UMAP visualization of integrated snRNAseq data sets displays (A) representation of each
804 storage condition in distinct clusters and (B) cell type diversity, each cluster is labeled by color. Samples
805 were integrated using harmony and UMAP was computed on the first 20 principal components after
806 highly variable gene selection. (C) Bar plots showing distribution of cell types from 3 snap frozen (S1-
807 3) and 2 RNA*later* (R1-2) and CellCover (CC) stored kidney biopsies.
808 Dot plot of select average gene expression values (log scale) and percentage of nuclei expressing
809 these genes within each cluster for known and newly discovered cell-type marker genes of (D) major
810 cell types of the kidney as well as of (E) 3 subtypes of proximal tubule cells, (F) 7 subtypes of
811 endothelial cells (EC 1-7) and of (FG 3 subtypes of immune cells (IMM) including t-cells (T-CELL) and
812 2 types of monocytes/macrophages (MAC-1, MAC-2).
813

814 **Fig. 4:** Comparison of cell type specific differential gene expression and cellular stress response
815 between sn RNAseq data sets of snap frozen, RNA*later* and CellCover stored pig kidney tissue. (A)
816 Cell type specific correlation of RNAlater and CellCover stored kidney biopsies with snap frozen kidney
817 biopsies. (B) Cell type specific differential up- and downregulated genes displayed on the x-axis for
818 RNAlater (orange) and CellCover (blue) stored kidney tissue compared to snap frozen kidney tissue.
819 Levels are calculated by Wilcoxon test (as implemented in Scanpy) with logFC = 1.5, FDR < 0.05 as

820 thresholds. (C) Replicability of glomerular cell types between snRNAseq data sets obtained from the
821 different cryopreservation conditions as defined by the area under the receiver operator characteristic
822 curve (AUROC) score. Podo: podocytes, gEC: glomerular endothelial cells, MC: mesangial cells. (D)
823 Comparison of activation of cellular stress response, apoptosis, hypoxia, and oxidative phosphorylation
824 between snRNAseq data sets from snap frozen, RNAlater and CellCover stored kidney tissue.
825 Activation status of each pathway was calculated with AUCell. (E) Violin plots showing the UMI counts
826 for canonical stress related genes in snRNAseq data sets from snap frozen, RNAlater and CellCover
827 stored kidney tissue
828
829 **Fig. 5:** UMAP visualization of 3 snRNAseq data sets from human kidney tissue stored in RNA*later*,
830 (A) after integration of 2 snRNAseq data sets from healthy controls and 1 data set from a clinically
831 indicated transplant kidney biopsy, (B) clustering into 12 distinct cell types of all major cell types of the
832 kidney. (C) Dot plot of cell-type defining marker genes.
833
834 **Fig. 6:** Proteome analysis of 4 kidney biopsies. (A) Distribution of protein abundances (LFQ normalized)
835 of each sample across the three storage methods. (B) PCA representation of the 12 samples across
836 the three methods. (C) Scores of cell type marker genes in proteomics data for the cell types detected
837 in snRNAseq data. The scores were calculated using the score_genes function in Scanpy using the
838 20 most significant genes with a positive log2FoldChange of 0.1 between cell types as cell type markers.
839 Significance calculations between methods were done using a two-sided t-test.

840 **Fig. 7:** Performance of snap frozen, RNAlater and CellCover stored kidney tissue in metabolome
841 analysis. (A) Principal component analysis of targeted lipid profiling: Each dot represents a sample with
842 their corresponding 95%-confidence interval as shaded area. Each storing condition were different from
843 each other. CellCover and RNA*later* harbored a higher variance than snap frozen and quality control
844 samples. Red: CellCover (n=3), blue: RNA*later* (n=3), turquoise: snap frozen (n=2), green: quality
845 control samples (n=3). Volcano plots of RNA*later* (B) and CellCover (C) compared to snap frozen kidney
846 biopsies. On the x-axis, the log_2-foldchanges are displayed, while negative log_{10}-p-values are displayed
847 on the y-axis. Dashed lines represent the cut-offs of 0.05 for p-value and 2 for fold change. Lipids
848 matching these cut-offs are labeled in blue if down regulated and in red when increased compared to

849 snap frozen. Lipids labeled in grey (b) had a fold change higher than 4 but a p-value between 0.05 and
850 0.1.

851 **Fig. 8:** Assessment of tissue architecture preservation (PAS-staining) and immunofluorescence
852 staining of RNAlater and CellCover stored kidney tissue compared to OCT-embedded tissue.
853 Immunofluorescence staining of nuclei (DAPI), basement membrane (Collagen 4), slit diaphragm
854 (Nephrin) and smooth muscle cells (α-SMA) of pig kidney tissue. PAS-Staining of RNAlater (A) and
855 CellCover (B) stored kidney tissue immediately frozen to -20°C. PAS-Staining of RNAlater (C) and
856 CellCover (D) stored kidney tissue at -80°C and OCT-embedded kidney tissue (E).
857 Immunofluorescence staining of RNAlater (F) and CellCover (G) stored kidney tissue immediately
858 frozen to -20°C and RNAlater (H) and CellCover (I) stored kidney tissue at -80°C and OCT-embedded
859 kidney tissue (J).

860

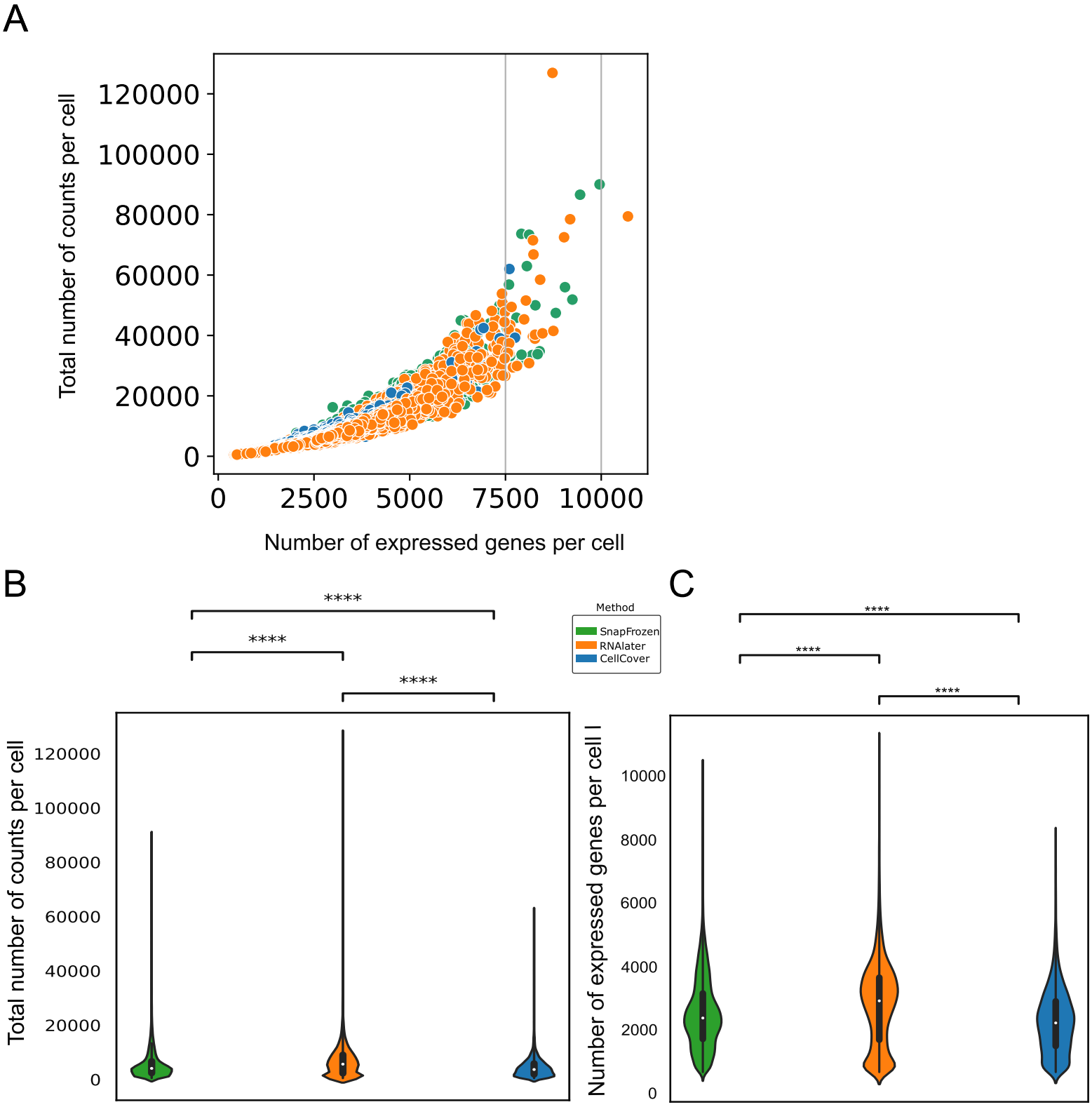
A
Total number of counts per cell
120000
100000
80000
60000
40000
20000
0
0
2500
5000
7500
10000
Number of expressed genes per cell
B
****
****
****
Method
SnapFrozen
RNAlater
CellCover
Total number of counts per cell
120000
100000
80000
60000
40000
20000
0
C
****
****
****
Number of expressed genes per cell l
10000
8000
6000
4000
2000
0

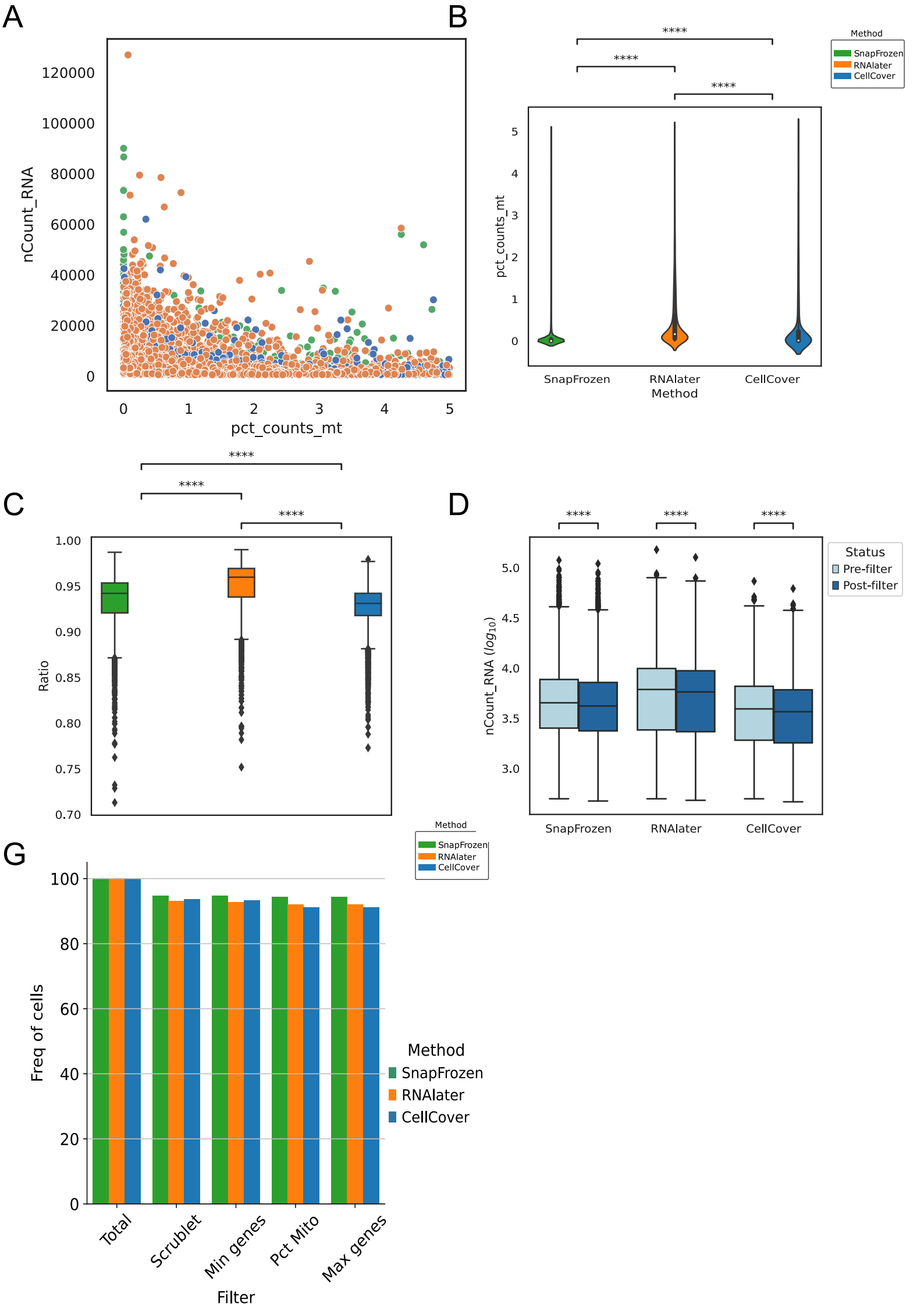
A
nCount_RNA
pct_counts_mt
B
Method
SnapFrozen
RNAlater
CellCover
****
pct_counts_mt
Method
C
Ratio
D
Status
Pre-filter
Post-filter
nCount_RNA (log_{10})
G
Freq of cells
Filter
Total
Scrublet
Min genes
Pct Mito
Max genes

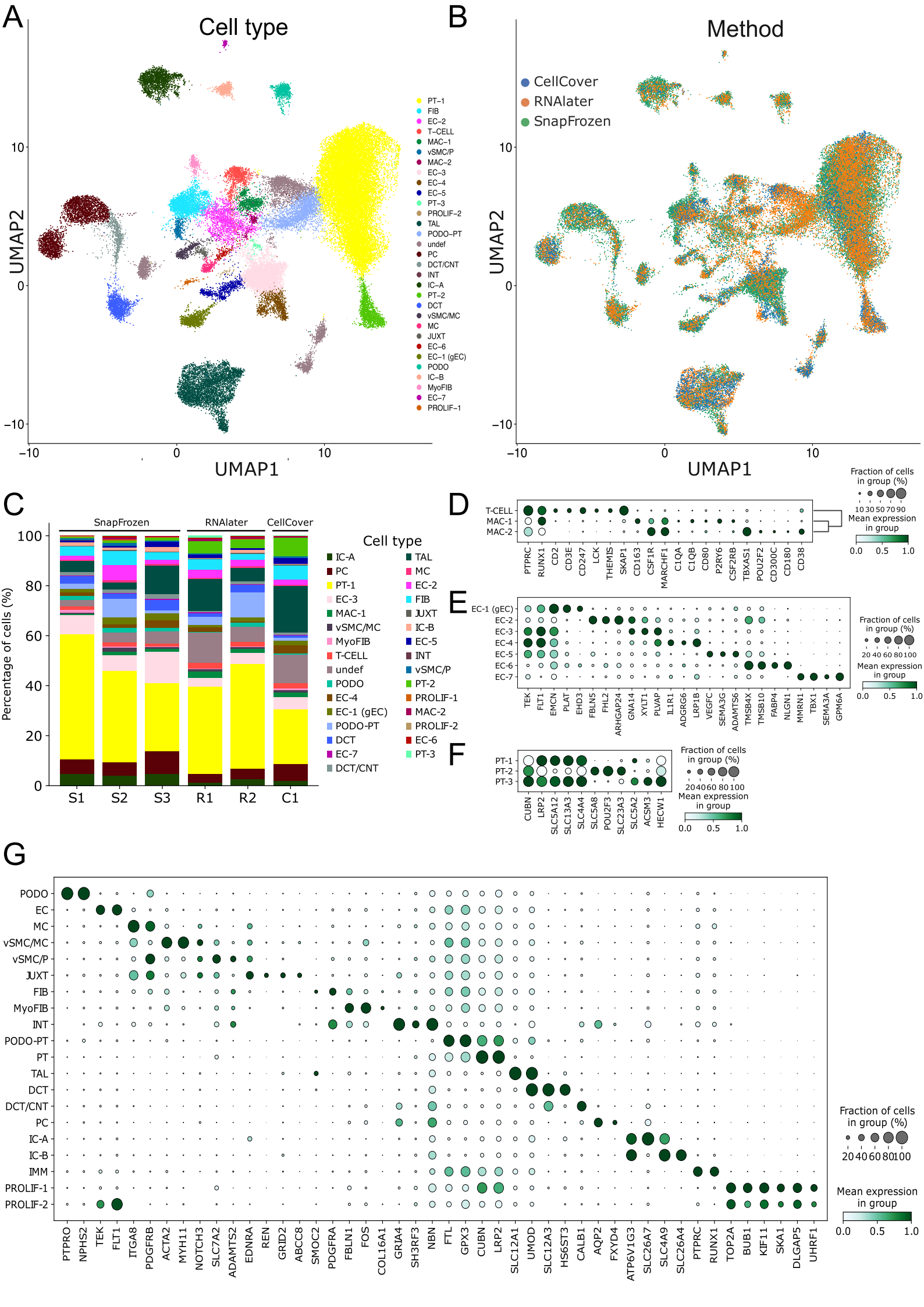
A
Cell type
UMAP2
UMAP1
PT-1
FIB
EC-2
T-CELL
MAC-1
vSMC/P
MAC-2
EC-3
EC-4
EC-5
PT-3
PROLIF-2
TAL
PODO-PT
undef
PC
DCT/CNT
INT
IC-A
PT-2
DCT
vSMC/MC
MC
JUXT
EC-6
EC-1 (gEC)
PODO
IC-B
MyoFIB
EC-7
PROLIF-1
B
Method
CellCover
RNAlater
SnapFrozen
C
SnapFrozen
RNAlater
CellCover
Percentage of cells (%)
S1
S2
S3
R1
R2
C1
Cell type
D
T-CELL
MAC-1
MAC-2
PTPRC
RUNX1
CD2
CD3E
CD247
LCK
THEMIS
SKAP1
CD163
CSF1R
MARCHF1
C1QA
C1QB
CD80
P2RY6
CSF2RB
TBXAS1
POU2F2
CD300C
CD180
CD38
Fraction of cells in group (%)
Mean expression in group
E
EC-1 (gEC)
EC-2
EC-3
EC-4
EC-5
EC-6
EC-7
TEK
FLT1
EMCN
PLAT
EHD3
FBLN5
FHL2
ARHGAP24
GNA14
XYLT1
PLVAP
IL1R1
ADGRG6
LRP1B
VEGFC
SEMA3G
ADAMTS6
TMSB4X
TMSB10
FABP4
NLGN1
MMRN1
TBX1
SEMA3A
GPM6A
F
PT-1
PT-2
PT-3
CUBN
LRP2
SLC5A12
SLC13A3
SLC4A4
SLC5A8
POU2F3
SLC23A3
SLC5A2
ACSM3
HECW1
G
PODO
EC
MC
vSMC/MC
vSMC/P
JUXT
FIB
MyoFIB
INT
PODO-PT
PT
TAL
DCT
DCT/CNT
PC
IC-A
IC-B
IMM
PROLIF-1
PROLIF-2
PTPRO
NPHS2
TEK
FLT1
ITGA8
PDGFRB
ACTA2
MYH11
NOTCH3
SLC7A2
ADAMTS2
EDNRA
REN
GRID2
ABCC8
SMOC2
PDGFRA
FBLN1
FOS
COL16A1
GRIA4
SH3RF3
NBN
FTL
GPX3
CUBN
LRP2
SLC12A1
UMOD
SLC12A3
HS6ST3
CALB1
AQP2
FXYD4
ATP6V1G3
SLC26A7
SLC4A9
SLC26A4
PTPRC
RUNX1
TOP2A
BUB1
KIF11
SKA1
DLGAP5
UHRF1

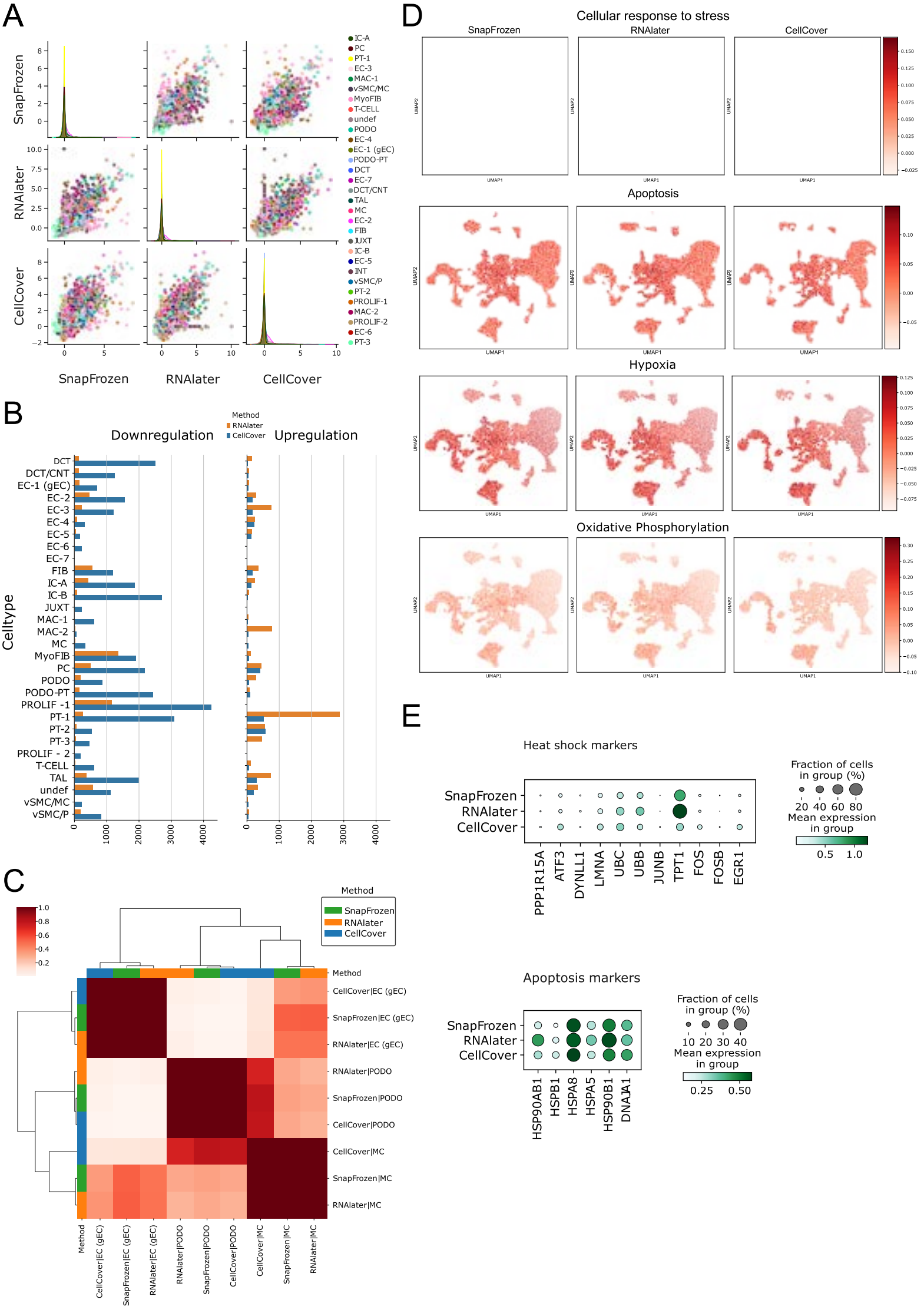
A
SnapFrozen
RNAlater
CellCover
IC-A
PC
PT-1
EC-3
MAC-1
vSMC/MC
MyoFIB
T-CELL
undef
PODO
EC-4
EC-1 (gEC)
PODO-PT
DCT
EC-7
DCT/CNT
TAL
MC
EC-2
FIB
JUXT
IC-B
EC-5
INT
vSMC/P
PT-2
PROLIF-1
MAC-2
PROLIF-2
EC-6
PT-3
B
Method
RNAlater
CellCover
Downregulation
Upregulation
Celltype
DCT
DCT/CNT
EC-1 (gEC)
EC-2
EC-3
EC-4
EC-5
EC-6
EC-7
FIB
IC-A
IC-B
JUXT
MAC-1
MAC-2
MC
MyoFIB
PC
PODO
PODO-PT
PROLIF -1
PT-1
PT-2
PT-3
PROLIF - 2
T-CELL
TAL
undef
vSMC/MC
vSMC/P
C
Method
SnapFrozen
RNAlater
CellCover
CellCover|EC (gEC)
SnapFrozen|EC (gEC)
RNAlater|EC (gEC)
RNAlater|PODO
SnapFrozen|PODO
CellCover|PODO
CellCover|MC
SnapFrozen|MC
RNAlater|MC
D
Cellular response to stress
SnapFrozen
RNAlater
CellCover
Apoptosis
Hypoxia
Oxidative Phosphorylation
UMAP1
UMAP2
E
Heat shock markers
SnapFrozen
RNAlater
CellCover
PPP1R15A
ATF3
DYNLL1
LMNA
UBC
UBB
JUNB
TPT1
FOS
FOSB
EGR1
Fraction of cells in group (%)
20 40 60 80
Mean expression in group
0.5 1.0
Apoptosis markers
HSP90AB1
HSPB1
HSPA8
HSPA5
HSP90B1
DNAJA1
Fraction of cells in group (%)
10 20 30 40
Mean expression in group
0.25 0.50

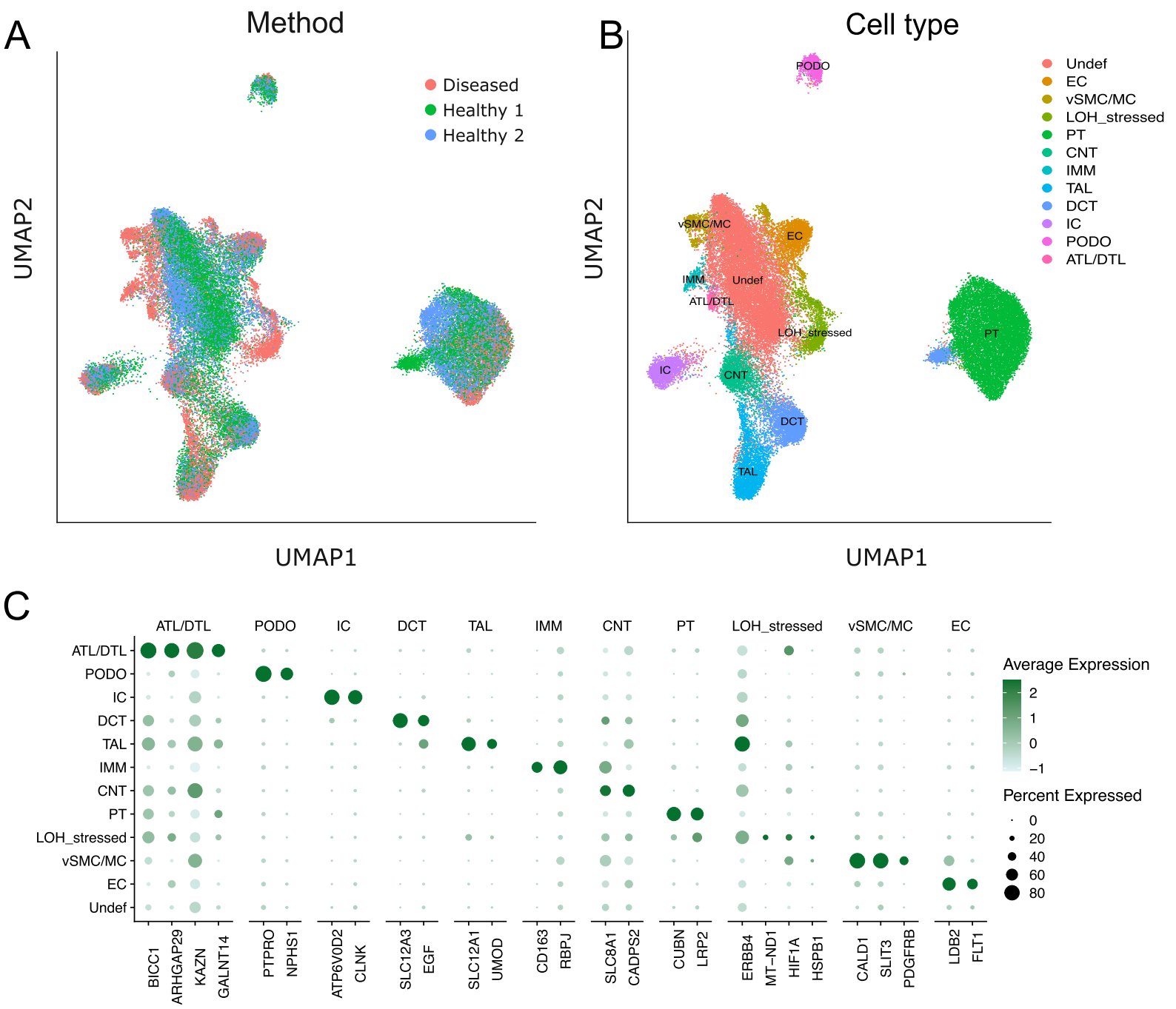
A
Method
Diseased
Healthy 1
Healthy 2
UMAP2
UMAP1
B
Cell type
Undef
EC
vSMC/MC
LOH_stressed
PT
CNT
IMM
TAL
DCT
IC
PODO
ATL/DTL
PODO
vSMC/MC
EC
IMM
Undef
ATL/DTL
LOH_stressed
PT
IC
CNT
DCT
TAL
UMAP2
UMAP1
C
ATL/DTL
PODO
IC
DCT
TAL
IMM
CNT
PT
LOH_stressed
vSMC/MC
EC
BICC1
ARHGAP29
KAZN
GALNT14
PTPRO
NPHS1
ATP6V0D2
CLNK
SLC12A3
EGF
SLC12A1
UMOD
CD163
RBPJ
SLC8A1
CADPS2
CUBN
LRP2
ERBB4
MT−ND1
HIF1A
HSPB1
CALD1
SLIT3
PDGFRB
LDB2
FLT1
Average Expression
2
1
0
−1
Percent Expressed
0
20
40
60
80

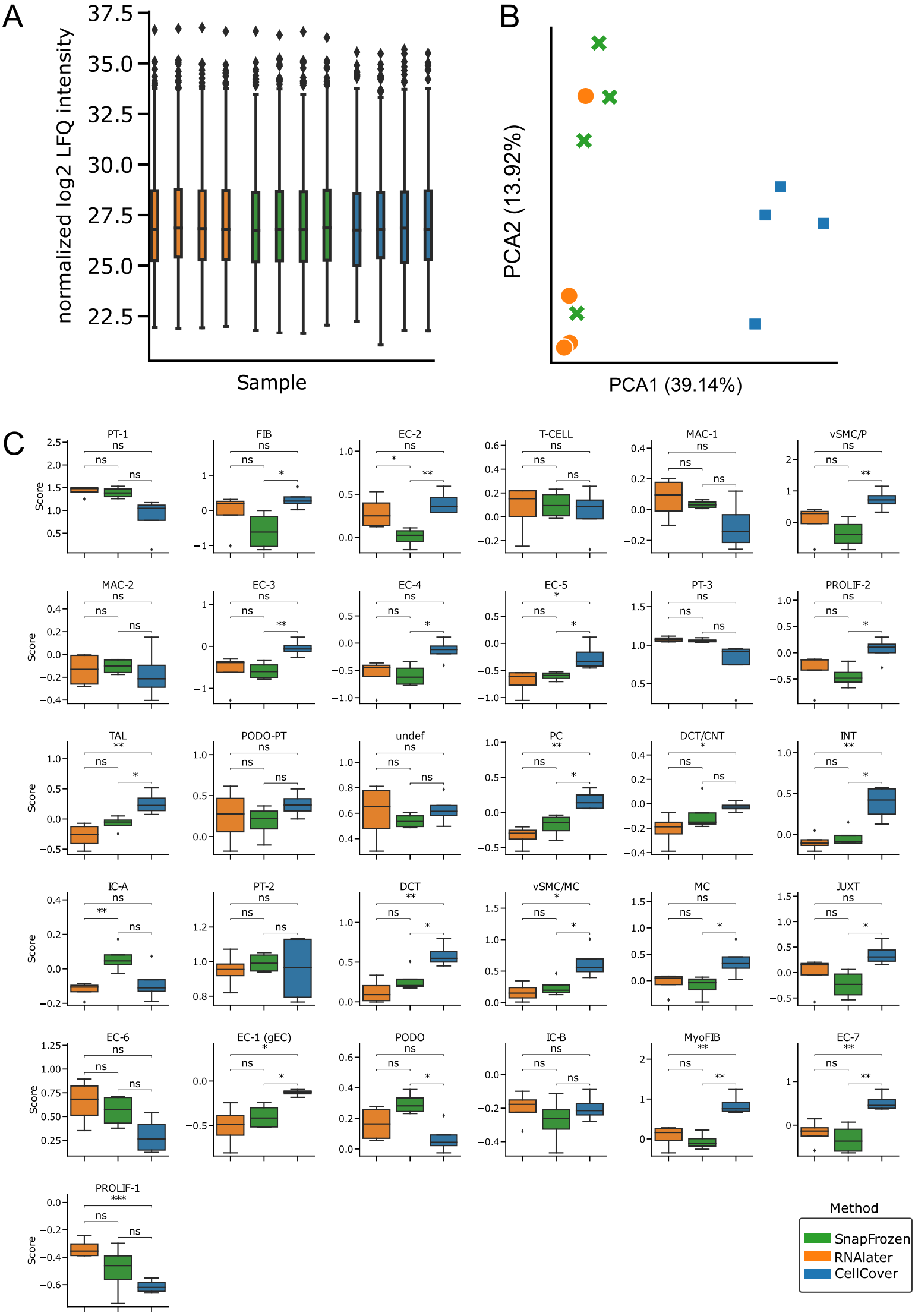
A
normalized log2 LFQ intensity
37.5
35.0
32.5
30.0
27.5
25.0
22.5
Sample
B
PCA2 (13.92%)
PCA1 (39.14%)
C
PT-1
FIB
EC-2
T-CELL
MAC-1
vSMC/P
MAC-2
EC-3
EC-4
EC-5
PT-3
PROLIF-2
TAL
PODO-PT
undef
PC
DCT/CNT
INT
IC-A
PT-2
DCT
vSMC/MC
MC
JUXT
EC-6
EC-1 (gEC)
PODO
IC-B
MyoFIB
EC-7
PROLIF-1
Score
ns
*
**
***
Method
SnapFrozen
RNAlater
CellCover

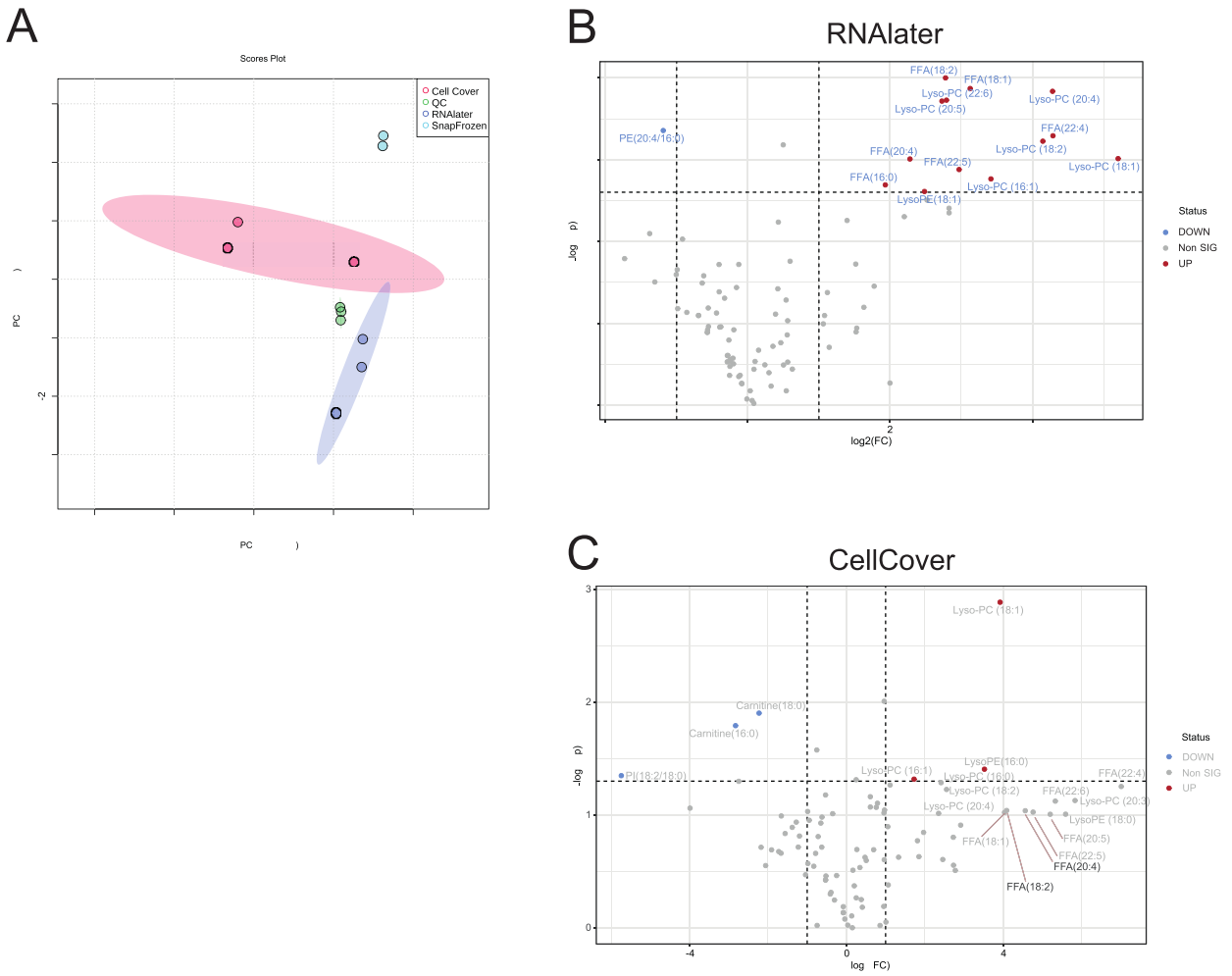
A
Scores Plot
Cell Cover
QC
RNAlater
SnapFrozen
PC
PC
B
RNAlater
FFA(18:2)
FFA(18:1)
Lyso-PC (22:6)
Lyso-PC (20:4)
Lyso-PC (20:5)
PE(20:4/16:0)
FFA(22:4)
Lyso-PC (18:2)
FFA(20:4)
FFA(22:5)
Lyso-PC (18:1)
FFA(16:0)
Lyso-PC (16:1)
LysoPE(18:1)
Status
DOWN
Non SIG
UP
-log p)
log2(FC)
C
CellCover
Lyso-PC (18:1)
Carnitine(18:0)
Carnitine(16:0)
LysoPE(16:0)
PI(18:2/18:0)
Lyso-PC (16:1)
FFA(22:4)
Lyso-PC (18:2)
FFA(22:6)
Lyso-PC (20:3)
Lyso-PC (20:4)
LysoPE (18:0)
FFA(18:1)
FFA(20:5)
FFA(22:5)
FFA(20:4)
FFA(18:2)
Status
DOWN
Non SIG
UP
-log p)
log FC)

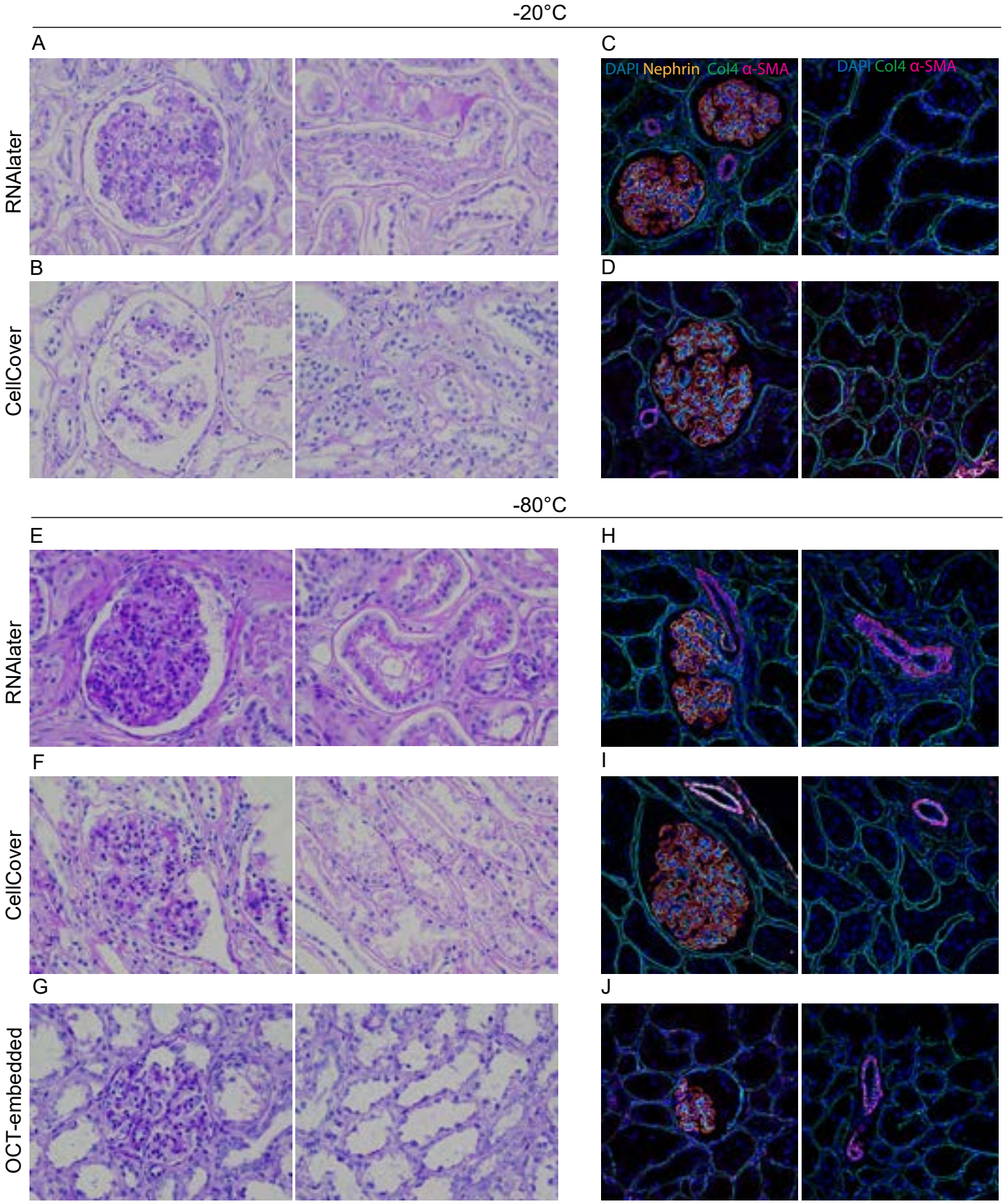
-20°C
A
C
DAPI Nephrin Col4 α-SMA
DAPI Col4 α-SMA
RNAlater
B
D
CellCover
-80°C
E
H
RNAlater
F
I
CellCover
G
J
OCT-embedded